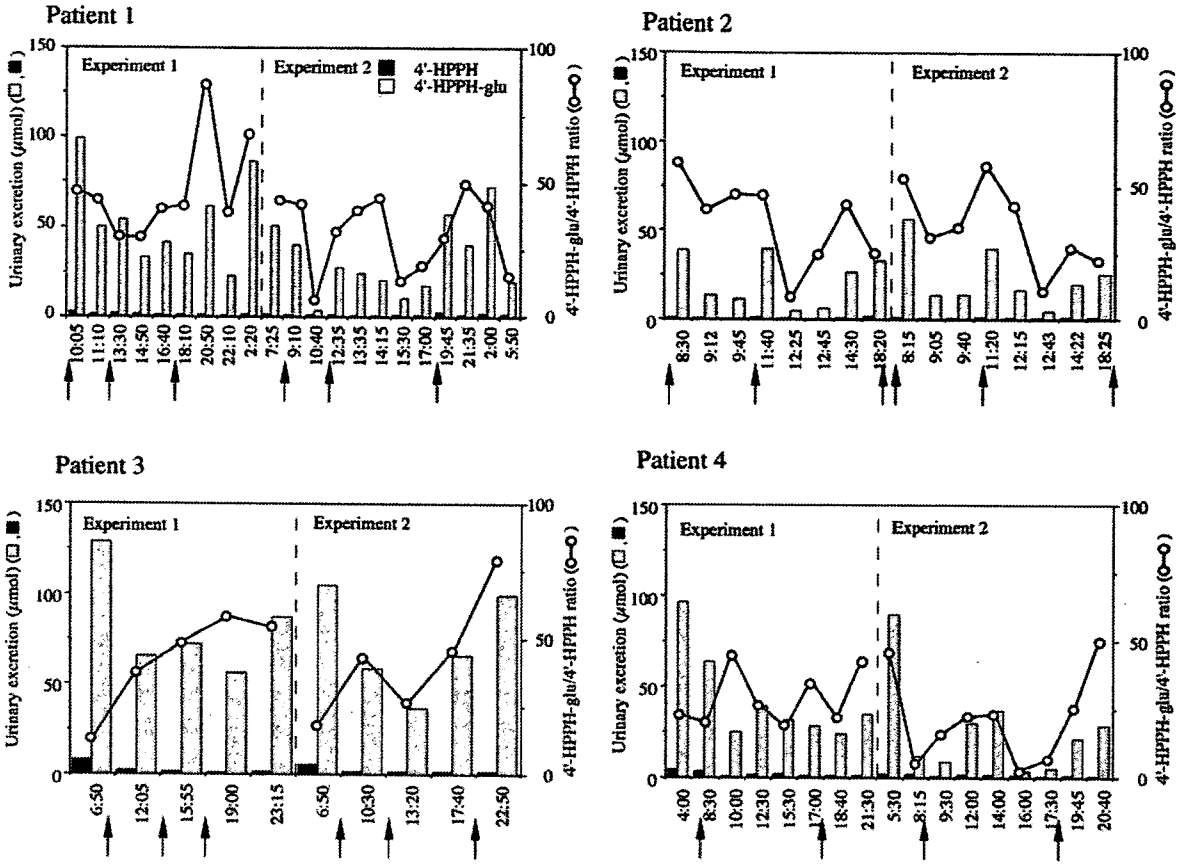

Fig. 2. Differences within a day in urinary excretion levels of 4′-HPPH and its *O*-glucuronide and their molar ratio. Urine samples were collected for 24 hr at various sampling times from 4 patients. Several days after experiment 1, the urine sampling for 24 hr was performed again in the same 4 patients for experiment 2. The ordinates represent the urinary excretion of 4′-HPPH and its *O*-glucuronide (left), and the molar ratio of 4′-HPPH *O*-glucuronide/4′-HPPH (right). The abscissa denotes the urine collection time. The arrows represent the administration time of phenytoin.

GT-3′

The underlined nucleotides indicate mismatched sites.

Statistical analyses: The relationships between the molar ratio of 4′-HPPH *O*-glucuronide/4′-HPPH and *UGT1A* genotype were investigated by Student's *t*-test.

Results

Excretion of 4′-HPPH and its *O*-glucuronide in urine at each sampling time: To evaluate the variability of the excretion levels of phenytoin metabolites during one day, urine samples were collected for 24 hr at various sampling times from 4 patients. Several days later, urine sampling for 24 hr was performed again in the same 4 patients (**Fig. 2**). The concentrations of 4′-HPPH and its *O*-glucuronide in the urine samples were measured by LC-MS/MS. The molar ratio of 4′-HPPH *O*-glucuronide/4′-HPPH was calculated as an index of the glucuronidation of 4′-HPPH. In patient 1, 4′-HPPH and its *O*-glucuronide were detected at 0.5–2.1 μmol and 3.1–86.6 μmol, respectively at different sampling times. It was confirmed that 4′-HPPH *O*-glucuronide was a major metabolite in human urine. The molar ratio of 4′-HPPH *O*-glucuronide/4′-HPPH in patient 1 differed by 3.6–87.6. Similarly, in patients 2, 3, and 4, the molar ratio of 4′-HPPH *O*-glucuronide/4′-HPPH ranged from 10.5–63.4, 16.5–95.7, and 2.9–51.1, respectively. Thus, during one day large differences in the excretion level of 4′-HPPH *O*-glucuronide and the molar ratio of 4′-HPPH *O*-glucuronide/4′-HPPH were observed. It was demonstrated that the excretion levels of 4′-HPPH and its *O*-glucuronide, and the molar ratio varied in each patient depending on the time of urine collection.

Inter-day differences in the 24-hr accumulated excretion levels of 4′-HPPH and its *O*-glucuronide in urine: Since there were large differences in the excretion level of 4′-HPPH and its *O*-glucuronide throughout the day, 24-hr accumulated urine samples were adopted to evaluate the variability of 4′-HPPH glucuronidation. The urine samples collected from a patient during 24 hr were combined. The 24-hr accumulated urine samples were obtained twice from 4 patients at intervals of sever-

al days. As shown in **Fig. 3**, the accumulated excretion levels of 4′-HPPH and its *O*-glucuronide showed similar values between the 2 samples in each patient. Furthermore, the molar ratio of 4′-HPPH *O*-glucuronide/4′-HPPH was also reproducible in each patient. Therefore, in the following study, interindividual differences in the glucuronidation of 4′-HPPH were evaluated with the molar ratio of 4′-HPPH *O*-glucuronide/4′-HPPH in the 24-hr accumulated urine samples.

Interindividual differences in the accumulated excretion levels of 4′-HPPH and its *O*-glucuronide in urine: In addition to the above 4 patients, 24-hr accumulated urine samples were collected from 11 patients. The volumes of the 24-hr accumulated urine in 15 patients ranged from 659 mL to 3,464 mL. The accumulated urinary excretion level of 4′-HPPH in 15 patients ranged from 0.7% (patient 5) to 5.7% (patient 7) of the daily dose of phenytoin (**Fig. 4A**). The accumulated urinary excretion level of 4′-HPPH *O*-glucuronide in 14 patients, excluding patient 5, ranged from 20.7% (patient 14) to 62.7% (patient 15) of the daily dose of phenytoin. In patient 5, the level was extremely low, 3.8%. In the 15 patients, the molar ratio of 4′-HPPH *O*-glucuronide/4′-HPPH ranged from 5.8 (patient 5) to 63.1 (patient 9) (**Fig. 4B**), showing a large, 11-fold interindividual difference. Patients 5 and 7 exhibited a lower molar ratio of 4′-HPPH *O*-glucuronide/4′-HPPH than the other patients.

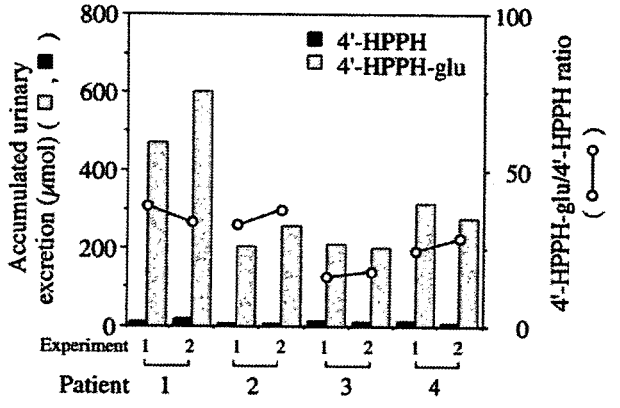

Fig. 3. Accumulated urinary excretion of 4′-HPPH and its *O*-glucuronide during 24 hr, and the molar ratio of 4′-HPPH *O*-glucuronide/4′-HPPH. Urine samples collected from a patient for 24 hr were combined. Urine samples were collected twice from 4 patients at intervals of several days.

Genotype of *CYP2C9*, *CYP2C19*, *UGT1A1*, *UGT1A6*, and *UGT1A9*: Genomic DNA was not available from patient 7. As shown in **Table 3**, patient 6 was genotyped as a heterozygote of *CYP2C9*3*. Patients 1 and 5 were genotyped as heterozygotes of *CYP2C19*2*. Patients 10 and 14 were genotyped as heterozygotes of *CYP2C19*3*. Concerning the genetic polymorphism of the *UGT1A1* gene, patient 1 and 13 were genotyped as a heterozygote of *UGT1A1*28* and *UGT1A1*60*. Patient 2 was genotyped as a heterozygote of *UGT1A1*28* and a homozygote of *UGT1A1*60*. Patients 4, 9, and 11 were heterozygotes of *UGT1A1*60*. Patients 15 was homozygotes of *UGT1A1*6*. Concerning the genetic polymorphism of the *UGT1A6* gene, patients 1 and 15 were homozygotes of *UGT1A6*2* and patients 2, 3, 9, 11, 12, and 13 were heterozygotes of *UGT1A6*2*. The *UGT1A9*4* and *UGT1A9*5* alleles were not found in the 14 patients. There was no significant difference in the molar ratio of 4′-HPPH *O*-glucuronide/4′-HPPH in the heterozygotes of *UGT1A1*28* (37.0±3.7, n=3) and the subjects who does not possessing the *UGT1A1*28* allele (27.3±18.3, n=11) ($p=0.394$). There was no significant differences between the ratios in the heterozygotes of *UGT1A1*60* (37.3±16.9, n=5) and those

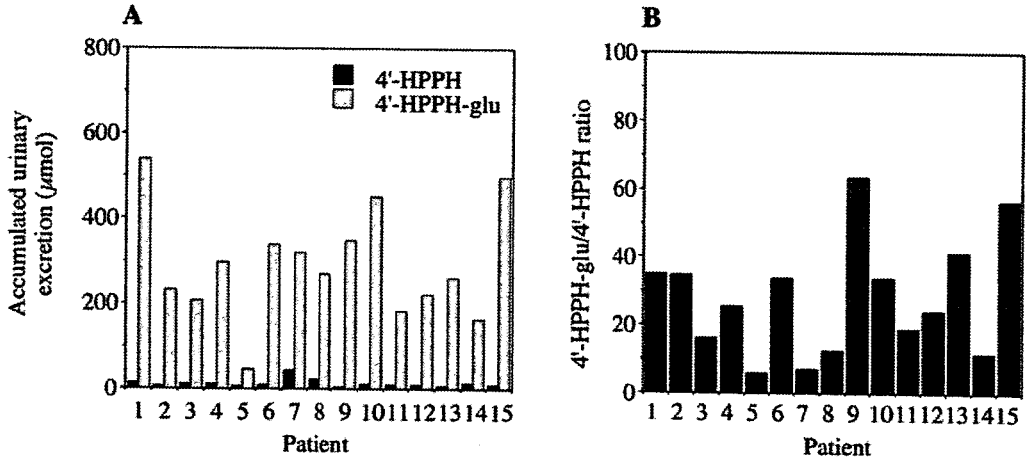

Fig. 4. Interindividual variability of 24-hr accumulated urinary excretion of 4′-HPPH and its *O*-glucuronide (A), and the molar ratio of 4′-HPPH-*O*-glucuronide/4′-HPPH (B). The 24-hr accumulated urine samples were collected from 15 patients who were administered phenytoin.

Table 3. Genotype of *CYP2C9*, *CYP2C19*, *UGT1A1*, *UGT1A6*, and *UGT1A9* genes in patients

Patient	*CYP2C9*3*	*CYP2C19*		*UGT1A1*									*UGT1A6*		*UGT1A9*	
		**2*	**3*	**6*	**7*	**25*	**27*	**28*	**29*	**38*	**60*	**62*	**2*	**3*	**4*	**5*
1	N	Hetero	N	N	N	N	N	Hetero	N	N	Hetero	N	Homo	N	N	N
2	N	N	N	N	N	N	N	Hetero	N	N	Homo	N	Hetero	N	N	N
3	N	N	N	N	N	N	N	N	N	N	N	N	Hetero	N	N	N
4	N	N	N	N	N	N	N	N	N	N	Hetero	N	N	N	N	N
5	N	Hetero	N	N	N	N	N	N	N	N	N	N	N	N	N	N
6	Hetero	N	N	N	N	N	N	N	N	N	N	N	N	N	N	N
7	—	—	—	—	—	—	—	—	—	—	—	—	—	—	—	—
8	N	N	N	N	N	N	N	N	N	N	N	N	N	N	N	N
9	N	N	N	N	N	N	N	N	N	N	Hetero	N	Hetero	N	N	N
10	N	N	Hetero	N	N	N	N	N	N	N	N	N	N	N	N	N
11	N	N	N	N	N	N	N	N	N	N	Hetero	N	Hetero	N	N	N
12	N	N	N	N	N	N	N	N	N	N	N	N	Hetero	N	N	N
13	N	N	N	N	N	N	N	Hetero	N	N	Hetero	N	Hetero	N	N	N
14	N	N	Hetero	N	N	N	N	N	N	N	N	N	N	N	N	N
15	N	N	N	Homo	N	N	N	N	N	N	N	N	Homo	N	N	N

N, no mutation; Hetero, heterozygous mutation; Homo, homozygous mutation.
—, Genomic DNA was not available from the patient 7.

in the subjects who dose not possessing the *UGT1A1*60* allele (24.4±16.3, n=8) ($p=0.199$). Concerning the *UGT1A6*2* allele, no significant difference was observed in the ratios in the homozygous *UGT1A6*2* (47.7, n=2), the heterozygous *UGT1A6*2* (33.0±17.6, n=6), and the homozygous wild-type (20.4±12.1, n=6) ($p=0.179$).

Discussion

In the present study, urinary excretion levels of 4′-HPPH and its *O*-glucuronide in patients who were taking phenytoin were determined to evaluate the interindividual difference in the glucuronidation of 4′-HPPH. Phenytoin is metabolized to 4′-HPPH by CYP2C9 and to a minor extent by CYP2C19.[4,5] There are genetic polymorphisms in *CYP2C9* and *CYP2C19* genes. Twelve and 19 polymorphic alleles have been reported for the *CYP2C9* and *CYP2C19* genes, respectively. Concerning the polymorphism of the *CYP2C9* gene in Japanese, *CYP2C9*3* has been found with the allele frequency of 0.018.[17] For the *CYP2C19* gene, the two alleles *CYP2C19*2* and *CYP2C19*3* can account for >99% of the defective alleles in oriental populations.[18] Therefore, we also determined these *CYP2C9* and *CYP2C19* alleles in the patients.

First, the large variation within a day in the urinary excretion levels of 4′-HPPH and its *O*-glucuronide was demonstrated. Therefore, the 24-hr accumulated urinary excretion levels of phenytoin metabolites were measured to evaluate the inter-day and interindividual differences in the glucuronidation of 4′-HPPH. In general, the ratio of the concentration of a metabolite to the unchanged drug has been employed to investigate the metabolic capacity in population studies. Accordingly, the molar ratio of 4′-HPPH *O*-glucuronide/4′-HPPH was calculated as an index of the glucuronidation of 4′-HPPH. In 15 patients, a large interindividual difference (11-fold) in the molar ratio of 4′-HPPH *O*-glucuronide/4′-HPPH was observed. This result was similar to that of our previous study that showed 28-fold interindividual differences in the 4′-HPPH glucuronide formation in microsomes from 14 human livers.[10]

Previously, we found that the glucuronidation of 4′-HPPH is catalyzed by multiple UGT1As of UGT1A1, UGT1A4, UGT1A6, and UGT1A9.[10] The genetic polymorphisms of the *UGT1A1*, *UGT1A6*, and *UGT1A9* genes have been reported (http://som.flinders.edu.au/FUSA/ClinPharm/UGT/). In the Japanese population, 9 alleles of the *UGT1A1* gene (*UGT1A1*6*, *UGT1A1*7*, *UGT1A1*25*, *UGT1A1*27*, *UGT1A1*28*, *UGT1A1*29*, *UGT1A1*38*, *UGT1A1*60*, and *UGT1A1*62*) and 2 alleles of the *UGT1A9* gene (*UGT1A9*4* and *UGT1A9*5*) have been found.[16,19-25] In Asian populations, the *UGT1A6*2* and *UGT1A6*3* alleles have been found.[26] These alleles have been reported to show decreased enzymatic activity of UGT.[20-23,27-30] Therefore, we investigated whether our patients possess these alleles. However, there was no relationship between the genetic polymorphisms of the UGT1A genes investigated in the present study and the interindividual differences in the 4′-HPPH *O*-glucuronide/4′-HPPH ratio. In the present study, the sample size might be small to detect the association between the genetic polymorphisms of the UGT1A and 4′-HPPH glucuronidation. Another possibility was that, even if a genetic polymorphism of one UGT1A isoform decreased the enzymatic activity, the other

UGT1A isoforms might compensate the 4′-HPPH glucuronosyltransferase activity.

In patient 5, the excretion level of 4′-HPPH *O*-glucuronide was extremely low. The patient was a heterozygote of *CYP2C19*2*. However, the other patients (patient number 1, 6, 10, and 14) who were also genotyped as heterozygotes of *CYP2C9*3*, *CYP2C19*2* or, *CYP2C19*3* showed normal excretion levels of 4′-HPPH *O*-glucuronide. Thus, the effects of the heterozygous mutation of *CYP2C9* or *CYP2C19* genes on the excretion level of 4′-HPPH and its *O*-glucuronide would be minor. In spite of the decreased metabolism of phenytoin to 4′-HPPH in patient 5, it was confirmed the excretion level of phenytoin in the patient was not very high, compared with the other patients (data not shown). Furthermore, the serum concentration of phenytoin was in the therapeutic range, 12.2 μg/mL, with the maintenance dose of 300 mg/day (**Table 1**). Although the possibility was suggested that phenytoin might be preferably metabolized to other metabolites such as 5-(3′-hydroxyphenyl)-5-phenylhydantoin, 5-(3′,4′-dihydroxyphenyl)-5-phenylhydantoin, or 5-(3′,4′-dihydroxy-1′,5′-cyclohexadien-1-yl)-5-phenylhydantoin,[31] it was confirmed that the concentrations of these minor metabolites in the urine sample were low by LC-MS/MS analysis (data not shown). Thus, the cause of the abnormal pharmacokinetics of phenytoin in the patient is unknown. In patient 5, sodium valproate was co-administered with phenytoin (**Table 1**). It is known that valproate affects the pharmacokinetics of phenytoin.[32,33] Valproate has been reported to competitively inhibit CYP2C9 catalyzed tolbutamide hydroxylase activity.[34] Furthermore, it has also been reported that valproate inhibits UGT1A9 catalyzed propofol glucuronidation.[35] Although the possibility of an interaction between valproate and phenytoin should be taken into consideration, it would not be enough to explain the abnormal excretion of 4′-HPPH *O*-glucuronide.

In conclusion, we found a large interindividual variability in the glucuronidation of 4′-HPPH in patients to whom phenytoin was administered was demonstrated. However, the variability was not related with the polymorphic mutations of the *UGT1A1*, *UGT1A6*, and *UGT1A9* genes. The variability might be affected by other factors except the genetic factor such as diet, environmental factors, state of disease, as that is generally accepted.[36] Since the large interindividual variability of 4′-HPPH glucuronidation may contribute to interindividual differences in toxic reactions to phenytoin or 4′-HPPH, the cause of the variability should be examined further.

Acknowledgments: This study was supported by a Grant-in-Aid for Encouragement of Young Scientists of the Ministry of Education, Science, Sports and Culture and a grant from Japan Research Foundation for Clinical Pharmacology. We acknowledge Mr. Brent Bell for reviewing the manuscript.

References

1) Hyson, C. and Sadler, M.: Cross sensitivity of skin rashes with antiepileptic drugs. *Can. J. Neurol. Sci.*, **24**: 245–249 (1996).
2) Odani, A., Hashimoto, Y., Otsuki, Y., Uwai, Y., Hattori, H., Furusho, K. and Inui, K.: Genetic polymorphism of the CYP2C subfamily and its effect on the pharmacokinetics of phenytoin in Japanese patients with epilepsy. *Clin. Pharmacol. Ther.*, **62**: 287–292 (1997).
3) Kutt, H. and Louis, S.: Anticonvulsant drugs. I. Pathophysiological and pharmacological aspects. *Curr. Ther.*, **13**: 113–131 (1972).
4) Bajpai, M., Roskos, L. K., Shen, D. D. and Levy, R. H.: Roles of cytochrome P4502C9 and P4502C19 in the stereoselective metabolism of phenytoin to its major metabolite. *Drug Metab. Dispos.*, **24**: 1401–1403 (1996).
5) Yasumori, T., Chen, L. S., Li, Q. H., Ueda, M., Tsuzuki, T., Goldstein, J. A., Kato, R. and Yamazoe, Y.: Human CYP2C-mediated stereoselective phenytoin hydroxylation in Japanese: difference in chiral preference of CYP2C9 and CYP2C19. *Biochem. Pharmacol.*, **57**: 1297–1303 (1999).
6) Maynert, E. W.: The metabolic fate of diphenylhydantoin in the dog, rat and man. *J. Pharmacol. Exp. Ther.*, **130**: 275–284 (1960).
7) Winn, L. M. and Wells, P. G.: Free radical-mediated mechanisms of anticonvulsant teratogenicity. *Eur. J. Neurol.*, **2**: 5–29 (1995).
8) Parman, T., Chen, G. and Wells, P. G.: Free radical intermediates of phenytoin and related teratogens. *J. Biol. Chem.*, **273**: 25079–25088 (1998).
9) Kim, P. M. and Wells, P. M.: Phenytoin-initiated hydroxyl radical formation: characterization by enhanced salicylate hydroxylation. *Mol. Pharmacol.*, **49**: 172–181 (1996).
10) Nakajima, M., Sakata, N., Ohashi, N., Kume, T. and Yokoi, T.: Involvement of mutiple UDP-glucuronosyltransferase 1A isoforms in glucuronidation of 5-(4′-hydroxyphenyl)-5-phenylhydantoin in human liver microsomes. *Drug Metab. Dispos.*, **27**: 1165–1170 (2002).
11) Buchanan, R. A. and Allen, R. J.: Diphenylhydantoin (Dilantin) and phenobarbital blood levels in epileptic children. *Neurology*, **21**: 866–871 (1971).
12) Caraco, Y., Muszkat, M. and Wood, A. J. J.: Phenytoin metabolic ratio: a putative marker of CYP2C9 activity *in vivo*. *Pharmacogenetics*, **11**: 587–596 (2001).
13) Pirmohamed, M., Alfirevic, A., Vilar, J., Stalford, A., Wilkins, E. G. L., Sim, E. and Park, B. K.: Association analysis of drug metabolizing enzyme gene polymorphisms in HIV-positive patients with co-trimoxazole hypersensitivity. *Pharmacogenetics*, **10**: 705–713 (2000).
14) Morais, S. M., Wilkinson, G. R., Blaisdell, J., Meyer, U. A., Nakamura, K. and Goldstein, J. A.: Identification of a new genetic defect responsible for the polymor-

phism of (*S*)-mephenytoin metabolism in Japanese. *Mol. Pharmacol.*, **46**: 594–598 (1994).
15) Morais, S. M., Wilkinson, G. R., Blaisdell, J., Nakamura, K., Meyer, U. A. and Goldstein, J. A.: The major genetic defect responsible for the polymorphism of *S*-mephenytoin metabolism in humans. *J. Biol. Chem.*, **269**: 15419–15422 (1994).
16) Ando, Y., Saka, H., Ando, M., Sawa, T., Muro, K., Ueoka, H., Yokoyama, A., Saitoh, S., Shimokata, K. and Hasegawa, Y.: Polymorphisms of UDP-glucuronosyltransferase gene and irinotecan toxicity: a pharmacogenetic analysis. *Cancer Res.*, **60**: 6921–6926 (2000).
17) Imai, J., Ieiri, I., Mamiya, K., Miyahara, S., Furuumi, H., Nanba, E., Yamane, M., Fukumaki, Y., Ninomiya, H., Tashiro, N., Otsubo, K. and Higuchi, S.: Polymorphism of the cytochrome P450 (CYP) 2C9 gene in Japanese epileptic patients: genetic analysis of the CYP2C9 locus. *Pharmacogenetics*, **10**: 85–89 (2000).
18) Ibeanu, G. C., Blaisdell, J., Ferguson, R. J., Ghanayem, B. I., Brosen, K., Benhamou, S., Bouchardy, C., Wilkinson, G. R., Dayer, P. and Goldstein, J. A.: A novel transversion in the intron 5 donor splice junction of CYP2C19 and a sequence polymorphism in exon 3 contribute to the poor metabolizer phenotype for the anticonvulsant drug *S*-mephenytoin. *J. Pharmacol. Exp. Ther.*, **290**: 635–640 (1999).
19) Mamiya, K., Ieiri, I., Shimamoto, J., Yukawa, E., Imai, J., Ninomiya, H., Yamada, H., Otsubo, K., Higuchi, S. and Tashiro, N.: The effects of genetic polymorphisms of CYP2C9 and CYP2C19 on phenytoin metabolism in Japanese adult patients with epilepsy: studies in stereoselective hydroxylation and population pharmacokinetics. *Epilepsia*, **39**: 1317–1323 (1998).
20) Aono, S., Adachi, Y., Uyama, E., Yamada, Y., Keino, H., Nanno, T., Koiwai, O. and Sato, H.: Analysis of genes for bilirubin UDP-glucuronosyltransferase in Gilbert's syndrome. *Lancet*, **345**: 958–959 (1995).
21) Koiwai, O., Aono, S., Adachi, Y., Kamisako, T., Yasui, M., Nishizawa, M. and Sato, H.: Crigler-Najjar syndrome type II is inherited both as a dominant and as a recessive trait. *Hum. Mol. Genet.*, **5**: 645–647 (1996).
22) Sumoto, R., Laosombat, V., Sadewa, A. H., Yokoyama, N., Nakamura, H., Matsuo, M. and Nishino, H.: Novel missense mutation of the UGT1A1 gene in Thai siblings with Gilbert's syndrome. *Pediatr. Int.*, **44**: 427–432 (2002).
23) Sugatani, J., Yamakawa, K., Yoshinari, K., Machida, T., Takagi, H., Mori, M., Kakizaki, S., Sueyoshi, T., Negishi, M. and Miwa, M.: Identification of a defect in the *UGT1A1* gene promoter and its association with hyperbilirubinemia. *Biochem. Biophys. Res. Commun.*, **292**: 492–497 (2002).
24) Saeki, M., Saito, Y., Jinno, H., Sai, K., Komamura, K., Ueno, K., Kamakura, S., Kitakaze, M., Shirao, K., Minami, H., Ohtsu, A., Yoshida, T., Saijo, N., Ozawa, S. and Sawada, J.: Three novel single nucleotide polymorphisms in UGT1A9. *Drug Metab. Pharmacokinet.*, **18**: 146–149 (2003).
25) Jinno, H., Saeki, M., Saito, Y., Tanaka-Kagawa, T., Hanioka, N., Sai, K., Kaniwa, N., Ando, M., Shirao, K., Minami, H., Ohtsu, A., Yoshida, T., Saijo, N., Ozawa, S. and Sawada, J.: Functional characterization of human UDP-glucuronosyltransferase 1A9 variant, D256N, found in Japanese cancer patients. *J. Pharmacol. Exp. Ther.*, **306**: 688–693 (2003).
26) Lampe, J. W., Bigler, J., Horner, N. K. and Potter, J. D.: UDP-glucuronosyltransferase (*UGT1A1*28* and *UGT1A6*2*) polymorphisms in Caucasians and Asians: relationships to serum bilirubin concentrations. *Pharmacogenetics*, **9**: 341–349 (1999).
27) Koiwai, O., Nishizawa, M., Hasada, K., Aono, S., Adachi, Y., Mamiya, N. and Sato, H.: Gilbert's syndrome is caused by a heterozygous missense mutation in the gene for bilirubin UDP-glucuronosyltransferase. *Hum. Mol. Genet.*, **4**: 1183–1186 (1995).
28) Yamamoto, K., Sato, H., Fujiyama, Y., Doida, Y. and Banba, T.: Contribution of two missense mutations (G71R and Y486D) of the bilirubin UDP glucuronosyltransferase (UGT1A1) gene to phenotypes of Gilbert's syndrome and Crigler-Najjar syndrome type II. *Biochim. Biophys. Acta*, **1406**: 267–273 (1998).
29) Bosma, P. J., Chowdhury, J. R., Bakker, C., Gantla, S., de Boer, A., Oostra, B. A., Lindhout, D., Tytgat, G. N. J., Jansen, P. L. M., Oude Elferink, R. P. J. and Chowdhury, N. R.: The genetic basis of the reduced expression of bilirubin UDP-glucuronosyltransferase 1 in Gilbert's syndrome. *N. Engl. J. Med.*, **333**: 1171–1175 (1995).
30) Ciotti, M., Marrone, A., Potter, C. and Owens, I. S.: Genetic polymorphism in the human UGT1A6 (planar phenol) UDP-glucuronosyltransferase: pharmacological implications. *Pharmacogenetics*, **7**: 485–495 (1997).
31) Komatsu, T., Yamazaki, H., Asahi, S., Gillam, E. M. J., Guengerich, F. P., Nakajima, M. and Yokoi, T.: Formation of a dihydroxy metabolite of phenytoin in human liver microsomes/cytosol: roles of cytochromes P450 2C9, 2C19, and 3A4. *Drug. Metab. Dispos.*, **28**: 1361–1368 (2000).
32) Bruni, J., Gallo, J. M., Lee, C. S., Perchalski, R. J. and Wilder, B. J.: Interactions of valproic acid with phenytoin. *Neurology*, **30**: 1233–1236 (1980).
33) Perucca, E., Hebdige, S., Frigo, G. M., Gatti, G., Lecchini, S. and Crema, A.: Interaction between phenytoin and valproic acid: plasma protein binding and metabolic effects. *Clin. Pharmacol. Ther.*, **28**: 779–789 (1980).
34) Wen, X., Wang, J.-S., Kivistö, K. T., Neuvonen, P. J. and Backman, J. T.: *In vitro* evaluation of valproic acid as an inhibitor of human cytochrome P450 isoforms: preferential inhibition of cytochrome P450 2C9 (CYP2C9). *Br. J. Clin. Pharmacol.*, **52**: 547–553 (2001).
35) Ethell, B. T., Anderson, G. D. and Burchell, B.: The effect of valproic acid on drug and steroid glucuronidation by expressed human UDP-glucuronosyltransferases. *Biochem. Pharmacol.*, **65**: 1441–1449 (2003).
36) Burchell, B. and Coughtrie, M. W.: Genetic and environmental factors associated with variation of human xenobiotic glucuronidation and sulfation. *Environ. Health Perspect.*, **105**: 739–747 (1997).

0090-9556/05/3312-1811–1818$20.00
DRUG METABOLISM AND DISPOSITION

DMD 33:1811–1818, 2005

Vol. 33, No. 12
6254/3063240
Printed in U.S.A.

CYP2A6 AND CYP2B6 ARE INVOLVED IN NORNICOTINE FORMATION FROM NICOTINE IN HUMANS: INTERINDIVIDUAL DIFFERENCES IN THESE CONTRIBUTIONS

Hiroyuki Yamanaka, Miki Nakajima, Tatsuki Fukami, Haruko Sakai, Akiko Nakamura, Miki Katoh, Masataka Takamiya, Yasuhiro Aoki, and Tsuyoshi Yokoi

Drug Metabolism and Toxicology, Division of Pharmaceutical Sciences, Graduate School of Medical Science, Kanazawa University, Kanazawa, Japan (H.Y., M.N., T.F., H.S., A.N., M.K., T.Y.); and Department of Legal Medicine, Iwate Medical University School of Medicine, Morioka, Japan (M.T., Y.A.)

Received June 24, 2005; accepted August 31, 2005

ABSTRACT:

Nornicotine is an *N*-demethylated metabolite of nicotine. In the present study, human cytochrome P450 (P450) isoform(s) involved in nicotine *N*-demethylation were identified. The Eadie-Hofstee plot of nicotine *N*-demethylation in human liver microsomes was biphasic with high-affinity (apparent K_m = 173 ± 70 μM, V_{max} = 57 ± 17 pmol/min/mg) and low-affinity (apparent K_m = 619 ± 68 μM, V_{max} = 137 ± 6 pmol/min/mg) components. Among 13 recombinant human P450s expressed in baculovirus-infected insect cells (Supersomes), CYP2B6 exhibited the highest nicotine *N*-demethylase activity, followed by CYP2A6. The apparent K_m values of CYP2A6 (49 ± 12 μM) and CYP2B6 (550 ± 46 μM) were close to those of high- and low-affinity components in human liver microsomes, respectively. The intrinsic clearances of CYP2A6 and CYP2B6 Supersomes were 5.1 and 12.5 nl/min/pmol P450, respectively. In addition, the intrinsic clearance of CYP2A13 expressed in *Escherichia coli* (44.9 nl/min/pmol P450) was higher than that of CYP2A6 expressed in *E. coli* (2.6 nl/min/pmol P450). Since CYP2A13 is hardly expressed in human livers, the contribution of CYP2A13 to the nicotine *N*-demethylation in human liver microsomes would be negligible. The nicotine *N*-demethylase activity in microsomes from 15 human livers at 20 μM nicotine was significantly correlated with the CYP2A6 contents (r = 0.578, $p < 0.05$), coumarin 7-hydroxylase activity (r = 0.802, $p < 0.001$), and *S*-mephenytoin *N*-demethylase activity (r = 0.694, $p < 0.005$). The nicotine *N*-demethylase activity at 100 μM nicotine was significantly correlated with the CYP2B6 contents (r = 0.677, $p < 0.05$) and *S*-mephenytoin *N*-demethylase activities (r = 0.740, $p < 0.005$). These results as well as the inhibition analyses suggested that CYP2A6 and CYP2B6 would significantly contribute to the nicotine *N*-demethylation at low and high substrate concentrations, respectively. The contributions of CYP2A6 and CYP2B6 would be dependent on the expression levels of these isoforms in any human liver.

Over a billion people worldwide smoke tobacco. Smoking exerts complex central and peripheral nervous system, behavioral, cardiovascular, and endocrine effects in humans (Vial 1986; Benowitz, 1988). The addiction liability and pharmacological effects of smoking are due to nicotine. Pulmonary absorption of nicotine is extremely rapid, occurring at a rate similar to that after intravenous administration (Russell and Feyerabend, 1978). In humans, absorbed nicotine is rapidly and extensively metabolized and eliminated to urine (Benowitz, 1988).

Nicotine is mainly (70–80%) metabolized to cotinine (Fig. 1) by cytochrome P450 (P450) 2A6 in humans (Nakajima et al., 1996). Nicotine is also metabolized to nornicotine, via *N*-demethylation. In humans, 2 to 3% of nicotine is excreted as nornicotine in 24-h urine (Kyerematen et al., 1990; Yamanaka et al., 2004). Cundy and Crooks (1984) have reported that only small amounts of nornicotine (1.6%) were detected in 24-h urine after [^{14}C]nicotine was injected intraperitoneally into guinea pigs. After a single arterial dose of labeled nicotine in rats, it was found that nornicotine accounted for 8% of the total recovery of the administered dose in urine (Curvall and Kazemi Vala, 1993). Therefore, the metabolism of nicotine to nornicotine would be a relatively minor pathway in the systemic clearance of nicotine. However, experimental animal studies revealed that nornicotine is present in brain at significant levels (approximately 20% of the total amount of nicotine and its metabolites) (Nordberg et al., 1989; Plowchalk et al., 1992; Nyback et al., 1994; Crooks et al., 1997). The nornicotine concentration in brain was nearly equal to that of nicotine (Crooks et al., 1997). These data indicated that nornicotine is a major metabolite of nicotine in brain. The half-lives of nornicotine in human plasma and rat brain are 6-fold and 3-fold longer than those of nicotine, respectively (Kyerematen et al., 1990; Ghosheh et al., 1999). Since nornicotine is pharmacologically active (Zhang et al., 1990; Liu et al., 1993), it may contribute to the neuropharmacological effects of nicotine and tobacco usage.

In our recent study (Yamanaka et al., 2004), the urinary excretion profile of nicotine metabolites in subjects entirely lacking the *CYP2A6* gene (poor metabolizers) was determined. We found that the urinary

This study was supported in part by Philip Morris Incorporated and by Research Fellowships of the Japan Society for the Promotion of Science for Young Scientists.

Article, publication date, and citation information can be found at http://dmd.aspetjournals.org.

doi:10.1124/dmd.105.006254.

ABBREVIATIONS: P450, cytochrome P450; NPR, NADPH-cytochrome P450 reductase; HPLC, high performance liquid chromatography; LC-MS/MS, liquid chromatography-tandem mass spectrometry; CL_{int}, intrinsic clearance.

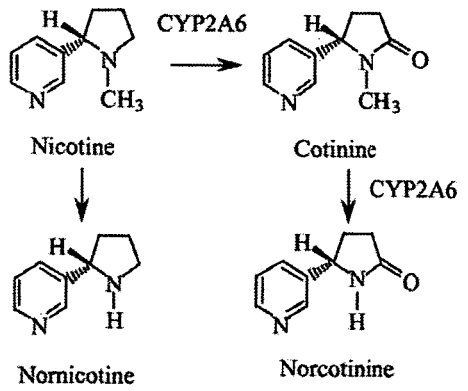

FIG. 1. Metabolic pathway of nicotine to cotinine, nornicotine, and norcotinine in humans.

excretion levels of nornicotine were similar between the poor metabolizers and extensive metabolizers who are homozygotes of the wild-type *CYP2A6* allele (Yamanaka et al., 2004), indicating the possibility that the enzyme responsible for the nornicotine formation might not be CYP2A6. In contrast, Murphy et al. (2005) recently reported that human CYP2A6 has a catalytic activity for nicotine *N*-demethylation. However, they did not investigate the other P450 isoforms. In the present study, we sought to identify the P450 isoform(s) involved in the nicotine *N*-demethylation to nornicotine in human liver microsomes.

Materials and Methods

Materials. Nicotine, nornicotine, and orphenadrine were purchased from Sigma-Aldrich (St. Louis, MO). Coumarin, quinidine, *S*-mephenytoin, and phenobarbital were purchased from Wako Pure Chemicals (Osaka, Japan). Nirvanol and ketoconazole were obtained from Ultrafine (Manchester, UK) and BIOMOL Research Laboratories (Plymouth Meeting, PA), respectively. $NADP^+$, glucose 6-phosphate, and glucose-6-phosphate dehydrogenase were purchased from Oriental Yeast Co. (Tokyo, Japan). Pooled human liver microsomes (H161), microsomes from 15 individual human livers (H003, H006, H023, H030, H043, H056, H064, H066, H070, H089, H093, H095, H112, HK23, and HK34), and recombinant human CYP1A1, CYP1A2, CYP1B1, CYP2A6, CYP2B6, CYP2C8, CYP2C9, CYP2C19, CYP2D6, CYP2E1, CYP3A4, CYP3A5, and CYP3A7 expressed in baculovirus-infected insect cells (Supersomes) were purchased from BD Gentest (Woburn, MA). All recombinant P450s were coexpressed with NADPH-P450 oxidoreductase. CYP2A6, CYP2B6, CYP2C8, CYP2C9, CYP2C19, CYP2E1, CYP3A4, and CYP3A7 were also coexpressed with cytochrome b_5. CYP1A2, CYP2A6, CYP2B6, CYP2D6, CYP2E1, and CYP3A4 protein contents in the microsomes of each human liver determined by immunoblot analyses were supplied by the manufacturer. The enzymatic activities for human P450 isoforms in each human liver microsome, including phenacetin *O*-deethylation (CYP1A2), coumarin 7-hydroxylation (CYP2A6), diclofenac 4′-hydroxylation (CYP2C9), *S*-mephenytoin 4′-hydroxylation (CYP2C19), bufuralol 1′-hydroxylation (CYP2D6), chlorzoxazone 6-hydroxylation (CYP2E1), and testosterone 6β-hydroxylation (CYP3A4), were also supplied by the manufacturer. Anti-human CYP2A6 monoclonal antibody, anti-human CYP2B6 monoclonal antibody, rabbit anti-human CYP2D6 serum, and rabbit anti-human CYP3A4 serum were obtained from Daiichi Pure Chemicals (Tokyo, Japan). It was reported by the manufacturer that these antibodies specifically react with each P450 isoform. All other chemicals and solvents were of the highest grade commercially available.

Construction of Expression Systems of CYP2A6 and CYP2A13 in *Escherichia coli*. A bicistronic construct consisting of the coding sequence of CYP2A6 followed by that of NADPH-cytochrome P450 reductase (NPR) was previously constructed in the pCW expression vector (Fukami et al., 2004). The full-length human CYP2A13 cDNA was obtained by polymerase chain reaction based on the reference sequence (GenBank accession number NM000766). A bicistronic construct consisting of the coding sequence of CYP2A13 followed by that of NPR was constructed using the CYP2A6/NPR expression vector. The 5′-terminus of CYP2A13 cDNA was modified to achieve a high expression level in a manner similar to that of the CYP2A6/NPR expression vector. Nucleotide sequences were confirmed by DNA sequence analysis (Long-Read Tower DNA sequencer; GE Healthcare, Little Chalfont, Buckinghamshire, UK). These plasmids were transformed to *E. coli* JM109. *E. coli* membranes expressing CYP2A6/NPR or CYP2A13/NPR were prepared, and the P450 content, protein concentration, and NADPH-cytochrome *c* reduction activity were determined according to the methods described previously (Fukami et al., 2004). P450s require a 1- to 3-fold excess amount of NPR to show the full activity in a reconstituted system (Soucek, 1999). The molar ratios of the NPR to the CYP2A6 and CYP2A13 were confirmed to be over 4 in the membrane preparations in the present study.

Preparation of Human Brain Microsomes from Striatum. This study was approved by the Ethics Committees of Iwate Medical University School of Medicine (Iwate, Japan) and Kanazawa University (Kanazawa, Japan). Human striatum samples (n = 3; 23, 79, and 82 years old) were obtained from autopsy materials that were discarded after pathological investigations. The postmortem delay was less than 24 h. After dissection, the samples were immediately frozen in liquid nitrogen and stored at −80°C. Microsomes were prepared as described by Voirol et al. (2000) with slight modifications, and were stored at −80°C until use.

Nicotine *N*-Demethylation Assays. The nicotine *N*-demethylase activity was determined by LC-MS/MS. A typical incubation mixture (200-μl total volume) contained 0.5 mg/ml human liver microsomes (or 20 pmol/ml Supersomes, 50 pmol/ml *E. coli* membrane, or 1 mg/ml human striatal microsomes), 50 mM potassium phosphate buffer (pH 7.4), an NADPH-generating system (0.5 mM $NADP^+$, 2 mM glucose 6-phosphate, 1 U/ml glucose-6-phosphate dehydrogenase, 4 mM $MgCl_2$), and nicotine (20 and 100 μM for human liver microsomes; 200 μM for recombinant P450s and human striatal microsomes). After a 2-min preincubation, the reactions were initiated by the addition of the NADPH-generating system and were incubated at 37°C for 20 min. The reactions were terminated by 100 μl of methanol. After centrifugation at 9000*g* for 5 min, the supernatant was filtered with a 0.22-μm filter (Ultrafree-MC centrifugal filter unit; Millipore Corporation, Eschborn, Germany). Aliquots of 5 μl were injected into the LC-MS/MS system.

LC-MS/MS Analysis. Nicotine and nornicotine were determined by LC-MS/MS as described previously (Yamanaka et al., 2004), with minor modifications. Liquid chromatography was performed using an HP 1100 system including a binary pump, an automatic sampler, and a column oven (Agilent Technologies, Waldbronn, Germany), which was equipped with a Develosil ODS-UG-3 (2.0 × 150 mm; Nomura Chemical, Aichi, Japan) column. The column temperature was 35°C. The mobile phase was 0.01% ammonia (A) and methanol (B). The conditions for elution were as follows: 20% B (0–0.5 min), 20 to 60% B (0.5–6 min), 60% B (6–10 min), 60 to 20% B (10–15 min). Linear gradients were used for all solvent changes. The flow rate was 0.2 ml/min. The liquid chromatograph was connected to a PE Sciex API 2000 tandem mass spectrometer (Applied Biosystems, Langen, Germany) operated in the positive electrospray ionization mode. The turbo gas was maintained at 550°C. Nitrogen was used as the nebulizing gas, turbo gas, and curtain gas at 50, 70, and 30 psi, respectively. Parent and/or fragment ions were filtered in the first quadrupole and dissociated in the collision cell using nitrogen as the collision gas. The collision energy ranged from 27 to 29 V. Two mass/charge (m/z) ion transitions were recorded in the multiple reaction monitoring mode: m/z 163 and 130 for nicotine, and m/z 149 and 80 for nornicotine. The retention times of nicotine and nornicotine were 13.0 min and 10.9 min, respectively (Fig. 2). Since nornicotine contaminants exist in the commercially available nicotine to the extent of ~0.25%, the content of nornicotine in the mixture incubated without the NADPH-generating system was subtracted to correct the activity.

Kinetic Analyses of Nicotine *N*-Demethylase Activities in Human Liver Microsomes or Recombinant P450 Isoforms. The kinetic studies were performed using pooled human liver microsomes or recombinant P450s. When determining the kinetic parameters, the substrate concentration ranged from 10 μM to 2000 μM for human liver microsomes, and from 10 μM to 1000 μM for recombinant P450s. The kinetic parameters were estimated from the fitted curves using a KaleidaGraph computer program (Abelbeck/Synergy, Reading, PA) designed for nonlinear regression analysis.

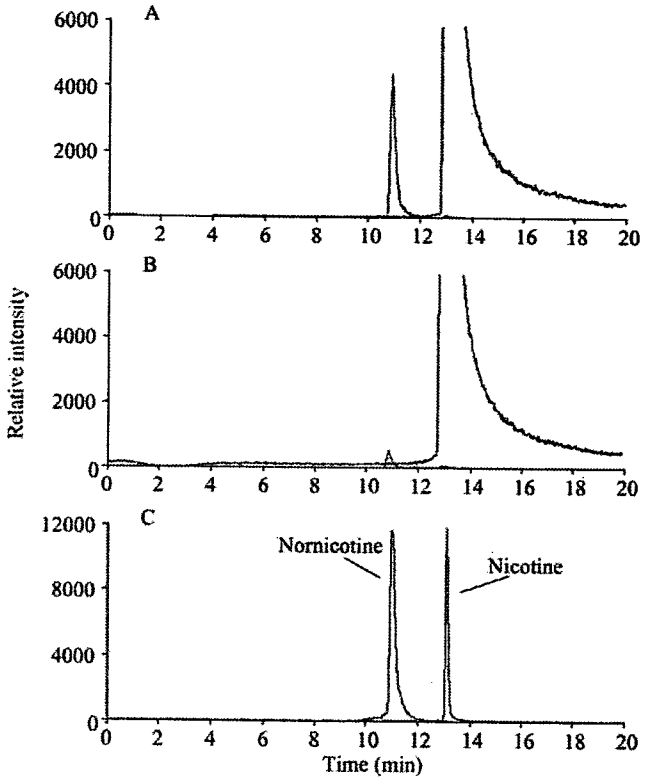

FIG. 2. Representative chromatograms of LC-MS/MS analysis of the nicotine N-demethylation in human liver microsomes. A and B, the incubation mixture including human liver microsomes and nicotine in the presence (A) or absence (B) of the NADPH-generating system. C, a mixture of authentic standards of nicotine and norcotinine (each 250 pg). Two mass/charge (*m/z*) ion transitions were recorded in the multiple reaction monitoring mode: *m/z* 163 and 130 for nicotine (13.0 min), and *m/z* 149 and 80 for nornicotine (10.9 min).

Inhibition Study. The nicotine *N*-demethylase activity in pooled human liver microsomes at 100 μM nicotine was determined in the presence of inhibitors for CYP2A6, CYP2B6, CYP2D6, or CYP3A4. Coumarin (100 μM), orphenadrine (500 μM), quinidine (10 μM), and ketoconazole (1 μM) were used as specific inhibitors for CYP2A6 (Yun et al., 1991), CYP2B6 (Reidy et al., 1989), CYP2D6 (Broly et al., 1989), and CYP3A4 (Newton et al., 1995), respectively. All inhibitors were dissolved in methanol so that the final concentration of solvent in the incubation mixture was <1%. For the inhibition study with coumarin, quinidine, and ketoconazole, the assays were performed as described above. For the inhibition study with orphenadrine (mechanism-based inhibitor), the incubation mixture including the inhibitor was preincubated in the presence of the NADPH-generating system at 37°C for 15 min and the reaction was initiated by the addition of nicotine. For the immunoinhibition study, the human liver microsomes (0.5 mg/ml) were incubated with anti-human CYP2A6 antibody (50 μl/mg), anti-human CYP2B6 antibody (50 μl/mg), anti-human CYP2D6 serum (50 μl/mg), or anti-human CYP3A4 serum (50 μl/mg) in 0.1 M potassium phosphate buffer (pH 7.4) on ice for 1 h. The nicotine *N*-demethylase activities were determined as described above. In addition, two samples of human liver microsomes, H003 (CYP2A6-abundant) and H112 (CYP2B6-abundant), were also used for the inhibition study of CYP2A6 and CYP2B6.

Prediction of the Percentage Contributions of CYP2A6 and CYP2B6 to Nicotine *N*-Demethylase Activity in Human Liver Microsomes. The percentage contributions of CYP2A6 and CYP2B6 to the nicotine *N*-demethylase activity (20 μM nicotine) were estimated based on the contents of these P450 isoforms in human liver microsomes determined by immunoblotting, based on the following equations (Becquemont et al., 1998): $V_{CYP2A6} = V_{rec\text{-}CYP2A6} \cdot A$ and $V_{CYP2B6} = V_{rec\text{-}CYP2B6} \cdot B$. *A* and *B* are the immunochemically determined CYP2A6 and CYP2B6 contents, respectively, in human liver microsomes. The $V_{rec\text{-}CYP2A6}$ and $V_{rec\text{-}CYP2B6}$ are the nicotine *N*-demethylase activities (20 μM nicotine) in recombinant CYP2A6 and CYP2B6, respectively. The contributions of CYP2A6 and CYP2B6 to the activity by human liver microsomes (V_{HL}) were calculated as follows: contribution of CYP2A6 (%) = (V_{CYP2A6}/V_{HL}) × 100 and contribution of CYP2B6 (%) = (V_{CYP2B6}/V_{HL}) × 100.

***S*-Mephenytoin *N*-Demethylation Assay.** *S*-Mephenytoin *N*-demethylase activity was determined by HPLC as described elsewhere (Ko et al., 1998) with minor modifications. A typical incubation mixture (200-μl total volume) contained 0.5 mg/ml human liver microsomal protein, 50 mM potassium phosphate buffer (pH 7.4), an NADPH-generating system, and 1 mM *S*-mephenytoin. After a 2-min preincubation, the reactions were initiated by the addition of the NADPH-generating system and were incubated at 37°C for 60 min. The reactions were terminated by 100 μl of ice-cold CH_3CN and added phenobarbital (25 ng) as an internal standard. The reaction mixtures were centrifuged at 9000*g* for 5 min, and aliquots of 100 μl were injected into the HPLC system.

HPLC analyses were performed using a PC-980 pump (Jasco, Tokyo, Japan), a UV-970 intelligent UV-visible detector (Jasco), an AS-950-10 autosampler (Jasco), a D-2500 integrator (Hitachi, Tokyo, Japan), and a CTO-6A column oven (Shimadzu, Kyoto, Japan) equipped with a Capcell PAK C18 UG120 (4.6 × 250 mm; 5 μm) column (Shiseido, Tokyo, Japan). The eluent was monitored at 204 nm. The mobile phase was 25% CH_3CN/50 mM potassium phosphate buffer (pH 3.8). The flow rate was 1.0 ml/min and the column temperature was 35°C. The retention times of nirvanol, phenobarbital, and *S*-mephenytoin were 9.5 min, 11.4 min, and 16.7 min, respectively. The quantification of nirvanol was performed by comparing the HPLC peak heights to those of an authentic standard with reference to an internal standard.

Statistical Analysis. Data are the mean of duplicate measurements. Correlations between the nicotine *N*-demethylase activity and immunoreactive P450 contents or enzymatic activities in microsomes from 15 human livers were determined by Pearson's product-moment method.

Results

Nicotine *N*-Demethylase Activity in Human Liver Microsomes. The formation of nornicotine from nicotine in the pooled human liver microsomes increased in protein concentration- and time-dependent manners. The formation was linear at least at 1 mg/ml microsomal protein and 30-min incubation. Unless specified, the standard incubation mixture containing 0.5 mg/ml microsomal protein was incubated at 37°C for 20 min. The kinetics of nicotine *N*-demethylation in the pooled human liver microsomes was biphasic (Fig. 3), indicating the involvement of multiple enzymes. The apparent K_m and V_{max} values for the high-affinity component were 173 ± 70 μM and 57 ± 17 pmol/min/mg, respectively. For the low-affinity component, the K_m was 619 ± 68 μM and the V_{max} was 137 ± 6 pmol/min/mg.

Nicotine *N*-Demethylase Activities by Recombinant P450 Isoforms. The nicotine *N*-demethylation was investigated in microsomes of baculovirus-infected insect cells expressing human P450s. As shown in Fig. 4A, CYP2B6 exhibited the highest nicotine *N*-demethylase activity (1.6 pmol/min/pmol P450), followed by CYP2A6 (0.3 pmol/min/pmol P450), CYP3A4 (0.2 pmol/min/pmol P450), and CYP2D6 (0.2 pmol/min/pmol P450). CYP1A1, CYP1A2, CYP2C8, CYP2C19, and CYP3A7 showed a trivial activity (0.02–0.11 pmol/min/pmol P450). Kinetic analyses were performed for the CYP2A6, CYP2B6, CYP2D6, and CYP3A4 Supersomes (Fig. 4B). The kinetics in recombinant CYP2B6 was fitted to the Michaelis-Menten plot, with apparent K_m = 550 ± 46 μM and V_{max} = 6.9 ± 0.3 pmol/min/pmol P450, resulting in the intrinsic clearance (CL_{int}) of 12.5 nl/min/pmol P450. The kinetics in recombinant CYP2A6 was also fitted to the Michaelis-Menten plot, with an apparent K_m = 49 ± 12 μM and V_{max} = 0.3 ± 0.0 pmol/min/pmol P450, resulting in CL_{int} of 5.1 nl/min/pmol P450. The activities in recombinant CYP2D6 and CYP3A4 were increased, with an increase in the concentration up to 1000 μM (0.6 and 0.3 pmol/min/pmol P450, respectively). The CL_{int} values calculated with the initial slope of the plots of *V* (velocity) versus *S*

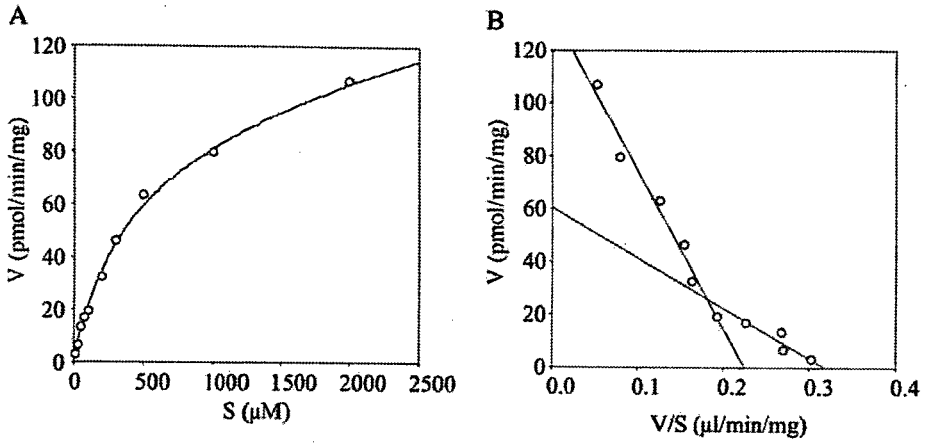

FIG. 3. Kinetic analyses of the nicotine *N*-demethylation in human liver microsomes. Michaelis-Menten (A) and Eadie-Hofstee plots (B) are shown. Pooled human liver microsomes were incubated with 10 to 2000 μM nicotine at 37°C for 20 min. Each data point represents the mean of duplicate determinations.

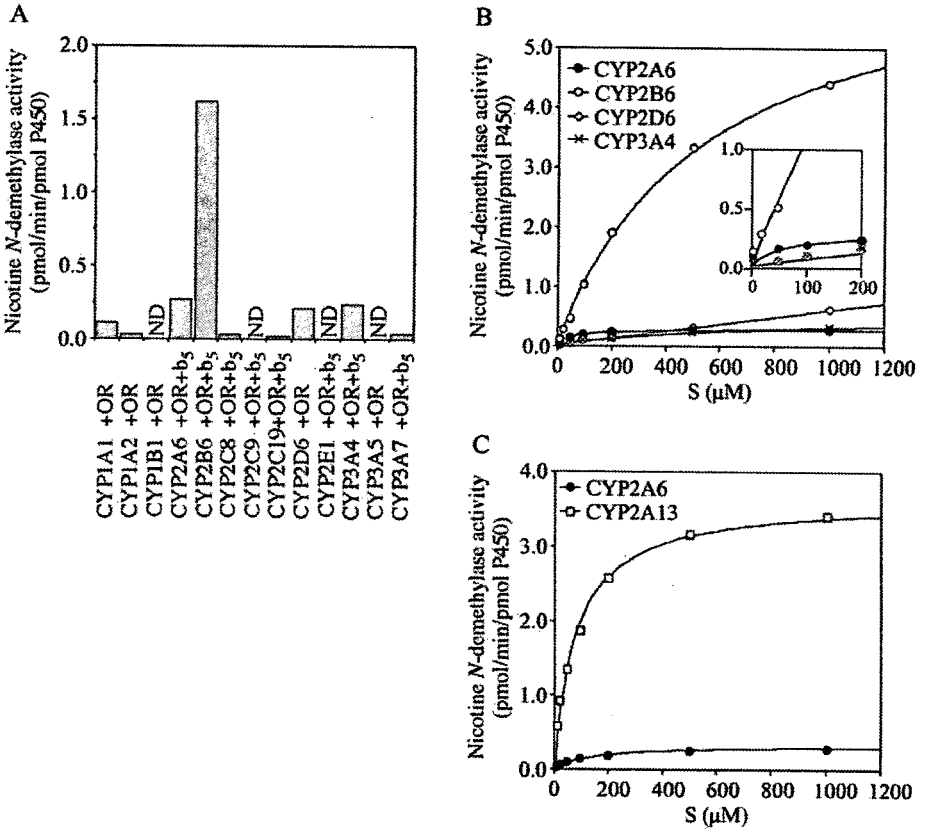

FIG. 4. Nicotine *N*-demethylase activities by recombinant human P450 isoforms. A, Nicotine *N*-demethylase activities by recombinant P450 isoforms expressed in baculovirus-infected insect cells (Supersomes) at 200 μM nicotine. Each column represents the mean of duplicate determinations. B, kinetic analyses of the nicotine *N*-demethylation by CYP2A6, CYP2B6, CYP2D6, and CYP3A4 Supersomes. C, kinetic analyses of the nicotine *N*-demethylation by recombinant CYP2A6 and CYP2A13 expressed in *E. coli*. The nicotine concentration ranged from 10 μM to 1000 μM. Each data point represents the mean of duplicate determinations. ND, not determined.

(substrate concentration) in recombinant CYP2D6 and CYP3A4 were both 0.7 nl/min/pmol P450, respectively.

Furthermore, kinetic analyses were performed for the recombinant CYP2A6 and CYP2A13 expressed in *E. coli* (Fig. 4C). The kinetics in recombinant CYP2A6 and CYP2A13 were also fitted to the Michaelis-Menten plot. The apparent K_m and V_{max} values were 129 ± 26 μM and 0.3 ± 0.0 pmol/min/pmol P450 for the recombinant CYP2A6, resulting in a CL_{int} of 2.6 nl/min/pmol P450. The apparent K_m and V_{max} values were 80 ± 11 μM and 3.7 ± 0.1 pmol/min/pmol P450 for the recombinant CYP2A13, resulting in a CL_{int} of 44.9 nl/min/pmol P450. Although CYP2A13 exhibited the highest CL_{int} of the nicotine *N*-demethylation, further analyses were not performed since this P450 isoform is hardly expressed in human liver microsomes.

Interindividual Variability in Nicotine *N*-Demethylase Activity in Microsomes from 15 Human Livers and Correlation Analyses. The nicotine *N*-demethylase activities in microsomes from 15 human livers were determined at substrate concentrations of 20 μM and 100 μM. The activities at 20 μM nicotine ranged from 0.6 to 9.7 pmol/min/mg, representing 16-fold variability. The activities at 100 μM

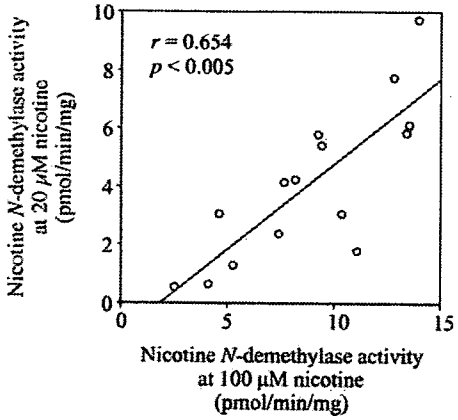

FIG. 5. Correlation analysis of the nicotine *N*-demethylase activities at two different substrate concentrations. The nicotine *N*-demethylase activities in microsomes from 15 human livers at 20 μM and 100 μM nicotine concentration were determined. Each data point represents the mean of duplicate determinations.

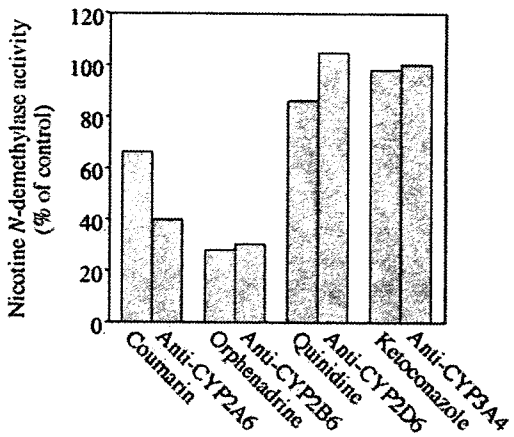

FIG. 6. Inhibitory effects of chemical inhibitors and antibodies against CYP2A6, CYP2B6, CYP2D6, or CYP3A4 on the nicotine *N*-demethylation in pooled human liver microsomes. The substrate concentration was 100 μM. Coumarin (100 μM), orphenadrine (500 μM), quinidine (10 μM), and ketoconazole (1 μM) were used as specific inhibitors for CYP2A6, CYP2B6, CYP2D6, and CYP3A4, respectively. For the immunoinhibition study, the human liver microsomes (0.5 mg/ml) were preincubated with antibodies against each P450 isoform (50 μl/mg) in 0.1 M potassium phosphate buffer (pH 7.4) on ice for 1 h. The nicotine *N*-demethylase activities were determined as described under *Materials and Methods*. The control activity in the pooled human liver microsomes was 16.5 pmol/min/mg protein. Each column represents the mean of duplicate determinations.

nicotine ranged from 2.5 to 14.0 pmol/min/mg (6-fold variability). A significant correlation ($r = 0.654$, $p < 0.005$) was observed between these activities at two different substrate concentrations (Fig. 5). As summarized in Table 1, the nicotine *N*-demethylase activity at 20 μM nicotine was significantly correlated with the CYP2A6 contents ($r = 0.578$, $p < 0.05$) and coumarin 7-hydroxylase activity ($r = 0.802$, $p < 0.001$) as the specific activity for CYP2A6. In addition, it was significantly correlated with the *S*-mephenytoin *N*-demethylase activity ($r = 0.694$, $p < 0.005$) as the specific activity for CYP2B6. The nicotine *N*-demethylase activity at 100 μM nicotine was significantly correlated with the CYP2B6 contents ($r = 0.677$, $p < 0.05$) and *S*-mephenytoin *N*-demethylase activities ($r = 0.740$, $p < 0.005$) as well as testosterone 6β-hydroxylase activity ($r = 0.523$, $p < 0.05$) as the specific activity for CYP3A4. No significant correlations were observed between the nicotine *N*-demethylase activities and the other activities or P450 isoform contents.

Inhibition Analyses. The effects of chemical inhibitors or antibodies against the P450 isoforms on the nicotine *N*-demethylase activities in pooled human liver microsomes were determined at 100 μM nicotine (Fig. 6). The activity was inhibited by coumarin (67% of the control activity), anti-CYP2A6 antibody (40% of the control activity), orphenadrine (28% of the control activity), and anti-CYP2B6 antibody (30% of the control activity). In contrast, the activity was not affected by quinidine, anti-CYP2D6 serum, ketoconazole, or anti-CYP3A4 serum.

Next, two samples of human liver microsomes, H003 (CYP2A6-abundant) and H112 (CYP2B6-abundant), were also used for the inhibition study of CYP2A6 and CYP2B6 (Table 2). The nicotine *N*-demethylase activity in human liver microsomal sample H003 (CYP2A6-abundant) at 20 μM nicotine was markedly inhibited by coumarin to 22% of the control activity and by anti-CYP2A6 antibody to 19% of the control activity. Orphenadrine and anti-CYP2B6 antibody moderately inhibited the activity (35 and 64% of control activity, respectively). The inhibition percentages for the nicotine *N*-demethylase activity at 100 μM nicotine by coumarin, anti-CYP2A6 antibody, and orphenadrine were almost the same as those at 20 μM nicotine. It is noteworthy that the activity was considerably inhibited by anti-CYP2B6 antibody (28% of control activity). The nicotine *N*-demethylase activity in human liver microsomal sample H112 (CYP2B6-abundant) at 20 μM nicotine was weakly inhibited by coumarin (81% of control activity) and anti-CYP2A6 antibody (53% of control activity). In contrast, the activity was markedly inhibited by orphenadrine and anti-CYP2B6 antibody (30% and 26% of control

TABLE 1

Correlation coefficients (r) between the nicotine N-demethylase activity and P450 contents or specific activities in 15 human liver microsomes

P450 Isoform	Nicotine *N*-Demethylase Activity (20 μM Nicotine)				Nicotine *N*-Demethylase Activity (100 μM Nicotine)			
	Protein Content[a]		Specific Activity[b]		Protein Content[a]		Specific Activity[b]	
	r	*p*	*r*	*p*	*r*	*p*	*r*	*p*
CYP1A2	−0.186	–[c]	−0.135	–	0.187	–	0.045	–
CYP2A6	0.578	<0.05	0.802	<0.001	0.202	–	0.430	–
CYP2B6	0.366	–	0.694	<0.005	0.677	<0.05	0.740	<0.005
CYP2C9	0.245	–	0.324	–	0.259	–	0.415	–
CYP2C19	−0.164	–	−0.144	–	0.245	–	0.032	–
CYP2D6	0.250	–	0.107	–	0.084	–	0.221	–
CYP2E1	0.404	–	0.097	–	0.354	–	0.032	–
CYP3A4	0.369	–	0.399	–	0.515	–	0.523	<0.05

[a] Protein contents of each P450 isoform were measured by immunoblot analyses.

[b] Phenacetin *O*-deethylase activity (CYP1A2), coumarin 7-hydroxylase activity (CYP2A6), *S*-mephenytoin *N*-demethylase activity (CYP2B6), diclofenac 4′-hydroxylase activity (CYP2C9), *S*-mephenytoin 4′-hydroxylase activity (CYP2C19), bufuralol 1′-hydroxylase activity (CYP2D6), chlorzoxazone 6-hydroxylase activity (CYP2E1), and testosterone 6β-hydroxylase activity (CYP3A4) were measured as specific activities for each P450 isoform.

[c] –, not significant.

TABLE 2

Inhibitory effects of chemical inhibitors and antibodies against CYP2A6 or CYP2B6 on the nicotine N-demethylase activity in human liver microsomes

Data are means of duplicate determinations. Values in parentheses are percentage of control activity.

Inhibitor or Antibody	H003		H112	
	20 μM Nicotine	100 μM Nicotine	20 μM Nicotine	100 μM Nicotine
	pmol/min/mg			
None	9.7 (100)	27.4 (100)	6.3 (100)	25.6 (100)
Coumarin (100 μM)	2.2 (22)	8.7 (32)	5.1 (81)	19.4 (76)
Anti-CYP2A6 (50 μl/mg)	1.8 (19)	7.0 (26)	3.3 (53)	13.8 (54)
Orphenadrine (500 μM)	3.4 (35)	11.1 (40)	1.9 (30)	6.9 (27)
Anti-CYP2B6 (50 μl/mg)	6.2 (64)	7.8 (28)	1.6 (26)	4.6 (18)

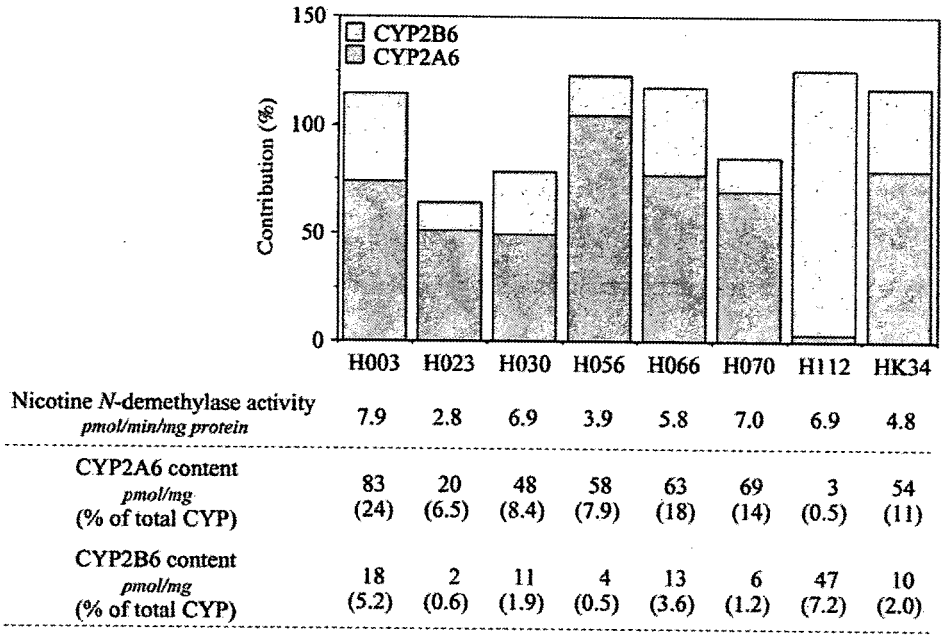

	H003	H023	H030	H056	H066	H070	H112	HK34
Nicotine *N*-demethylase activity *pmol/min/mg protein*	7.9	2.8	6.9	3.9	5.8	7.0	6.9	4.8
CYP2A6 content *pmol/mg* (% of total CYP)	83 (24)	20 (6.5)	48 (8.4)	58 (7.9)	63 (18)	69 (14)	3 (0.5)	54 (11)
CYP2B6 content *pmol/mg* (% of total CYP)	18 (5.2)	2 (0.6)	11 (1.9)	4 (0.5)	13 (3.6)	6 (1.2)	47 (7.2)	10 (2.0)

FIG. 7. The percentage contributions of CYP2A6 and CYP2B6 to the nicotine *N*-demethylation in human liver microsomes. The prediction method was based on the activities by recombinant P450s and the contents of each P450 isoform in human liver microsomes. The contributions of CYP2A6 and CYP2B6 in microsomes from eight human livers to nicotine *N*-demethylase activity at 20 μM nicotine concentration were determined. The total P450 contents determined by CO-difference spectrum and CYP2A6 or CYP2B6 protein contents determined by immunoblot analyses in each human liver microsome were supplied by the manufacturer.

activity, respectively). The nicotine *N*-demethylase activity at 100 μM nicotine was also inhibited to a similar extent.

Contributions of CYP2A6 and CYP2B6 to Nicotine *N*-Demethylase Activity in Human Liver Microsomes. The contributions of CYP2A6 and CYP2B6 to the nicotine *N*-demethylase activity in microsomes from eight human livers were determined. The nicotine *N*-demethylase activity in the human liver microsomes (H003, H023, H030, H056, H066, H070, H112 and HK34) at 20 μM nicotine ranged from 2.8 to 7.9 pmol/min/mg protein (Fig. 7). The immunochemically determined contents of CYP2A6 and CYP2B6 (pmol/mg) supplied by the manufacturer are shown in Fig. 7. The $V_{rec\text{-}CYP2A6}$ and $V_{rec\text{-}CYP2B6}$ values were 0.07 and 0.18 pmol/min/pmol P450, respectively. Consequently, the contributions of CYP2A6 and CYP2B6 to the nicotine *N*-demethylase activity in human liver microsomes that are relatively CYP2A6-abundant (those except H112) were estimated as 49 to 104% and 13 to 41%, respectively (Fig. 7). In contrast, the contributions of CYP2A6 and CYP2B6 in the human liver microsomal sample (H112), which is CYP2B6-abundant, were estimated as 3% and 123%, respectively. The sum of the percentages of the contributions of CYP2A6 and CYP2B6 ranged from 64% to 126%.

Nicotine *N*-Demethylase Activities in Human Brain Microsomes from Striatum. Nicotine *N*-demethylase activities in human brain microsomes from striatum were determined at 200 μM nicotine. One sample showed a distinct activity (0.9 pmol/min/mg), and the other two samples showed weak activities (0.1 pmol/min/mg). The expression of CYP2A6 and CYP2B6 mRNA in these striatum samples was confirmed with reverse transcription-polymerase chain reaction (data not shown).

Discussion

Recently, Murphy et al. (2005) detected the nornicotine formation from nicotine in recombinant CYP2A6 in baculovirus-infected insect cells with [^{3}H]nicotine. Although they reported that the formed nornicotine was about 5% of the total metabolism of nicotine (Murphy et al., 2005), the absolute activity was unknown. In the present study, we first determined the specific activity for the nicotine *N*-demethylation in recombinant CYP2A6 (Supersomes), and its CL_{int} was calculated as 5.1 nl/min/pmol P450. It is emphasized that recombinant CYP2B6 revealed a 2.5-fold higher CL_{int} than did CYP2A6. The K_m values in the recombinant CYP2A6 and CYP2B6 were close to those for the high- and low-affinity components, respectively, in human liver microsomes. At a relatively low substrate concentration (20 μM nicotine, lower than the K_m value for CYP2A6), the nicotine *N*-demethylase activity was significantly correlated with the content or specific

activity for CYP2A6. In addition, it was also correlated with the CYP2B6 specific activity. We confirmed that no significant correlation was observed between CYP2A6 and CYP2B6 in these specific activities and protein contents in the panel of human liver microsomes used in this study (data not shown). At a relatively high substrate concentration (100 μM), the nicotine *N*-demethylase activity was significantly correlated with the content or specific activity for CYP2B6. These results suggested that the contributions of CYP2A6 and CYP2B6 to the nicotine *N*-demethylation would be significant at low and high substrate concentrations, respectively.

Murphy et al. (2005) reported that CYP2A13 also could catalyze the nicotine *N*-demethylation more efficiently than CYP2A6, although the absolute enzymatic activities were not determined. In this study, we found that recombinant CYP2A13 exhibited a 17-fold higher CL_{int} value than recombinant CYP2A6 expressed in *E. coli*. However, it has been reported that the expression level of CYP2A13 mRNA (7 $\pm$ 6 attomoles/mg RNA) was much lower than that of CYP2A6 mRNA (13,000 $\pm$ 12,000 attomoles/mg RNA) in human livers (Su et al., 2000). Although we cannot quantify the expression levels of CYP2A13 and CYP2A6 proteins in human livers since antibodies specific for each isoform are not available, it is considered that the expression level of CYP2A13 protein would also be much lower than that of CYP2A6 protein. Thus, the role of CYP2A13 in the nornicotine formation would be mostly insignificant in human livers.

The nicotine *N*-demethylase activity in human liver microsomes at a nicotine concentration of 100 μM was also significantly correlated with the testosterone 6β-hydroxylase activity (the specific activity for CYP3A4). In the panel of human liver microsomes used in this study, a fortuitous correlation between the testosterone 6β-hydroxylase activity and CYP2B6 protein content ($r = 0.809$, $p < 0.001$) was also observed. Furthermore, the nicotine *N*-demethylase activity in human liver microsomes was not inhibited by ketoconazole and anti-CYP3A4 serum. These results suggested that the involvement of CYP3A4 in the nicotine *N*-demethylase activity in human liver microsomes would be negligible.

Quantitative analysis of the contributions of each P450 isoform using the activities by recombinant P450s and contents of each P450 isoform in human liver microsomes revealed that the contributions of CYP2A6 and CYP2B6 to the nicotine *N*-demethylation would be dependent on the individual expression levels of these isoforms. The sum of the percentage contributions of CYP2A6 and CYP2B6 ranged from 64% to 126%, indicating that these P450 isoforms are the major enzymes responsible for the nicotine *N*-demethylation in humans. One limitation of this prediction method is that the P450 contents were measured by immunoblot analysis. Immunoblot analysis cannot distinguish between active and inactive protein. Another prediction method is using the relative activity factor with specific activities for each P450 (Crespi, 1995; Nakajima et al., 1999). However, the relative activity factor method for predicting the CYP2B6 contribution was not successful (the estimated contributions of CYP2B6 in all human liver microsomes were over 100%), possibly because of the limited specificity of CYP2B6 substrates such as *S*-mephenytoin or benzyloxyresorufin (data not shown). The inhibition analyses with chemicals and antibodies against CYP2A6 and CYP2B6 in the present study would support the contributions of CYP2A6 and CYP2B6 to the nicotine *N*-demethylase activity in human liver microsomes.

Previously, we demonstrated that the urinary excretion levels of nornicotine in subjects entirely lacking the *CYP2A6* gene were similar to those in normal subjects, suggesting that the involvement of CYP2A6 in the nornicotine formation was slight (Yamanaka et al., 2004). However, the present in vitro study demonstrated that CYP2A6 has a significant catalytic activity for nornicotine formation as a high-affinity component. Therefore, the nornicotine formed in the subjects lacking CYP2A6 would result from the compensatory role of CYP2B6.

In the present study, the CL_{int} for the nornicotine formation in human liver microsomes was calculated as 0.3 μl/min/mg. Previously, we demonstrated that the CL_{int} for the cotinine formation in human liver microsomes was 1.6 μl/min/mg (Nakajima et al., 1996). The difference in the intrinsic clearances between the two metabolic pathways would reflect the metabolic profile of nicotine in human urine, i.e., nornicotine, 2 to 3%, and cotinine, 70 to 80% (Benowitz et al., 1994).

Nornicotine is a major metabolite of nicotine in brain (Crooks et al., 1997). In the human brain, CYP2B6 protein is expressed in various regions including the occipital cortex, hippocampus, striatum, cerebellar vermis, and cerebellar hemisphere (Gervot et al., 1999; Miksys et al., 2003). In addition, Miksys and Tyndale (2004) recently reported that CYP2A6 mRNA is also expressed in various regions of the human brain. In particular, the expression levels of CYP2B6 protein and CYP2A6 mRNA are high in the striatum (Miksys et al., 2003; Miksys and Tyndale 2004). These backgrounds prompted us to investigate the nicotine *N*-demethylase activities in human brain microsomes from striatum. Consequently, the nicotine *N*-demethylase activity was detected in human brain microsomes from striatum. The present study demonstrated that nornicotine in brain could have originated from the nicotine *N*-demethylation locally in the brain, in addition to the nornicotine that is formed in the liver and subsequently passes the blood-brain barrier. It has been reported that nicotine can induce CYP2B in rat brain (Anandatheerthavarada et al., 1993; Miksys et al., 2000). In smokers, a higher level of CYP2B6 protein in the brain was detected than in nonsmokers, suggesting that nicotine can also induce human CYP2B6 in the brain (Miksys et al., 2003). Until now, there has been no information on whether CYP2A6 is inducible by nicotine. Generally, the induction of CYP2B is mediated by constitutive androstane receptor or pregnane X receptor. These receptors usually cross talk with each other toward target genes. Recently, Lamba et al. (2004) reported that nicotine could activate human pregnane X receptor. Collectively, the induction of CYP2B6 by nicotine would enhance the metabolism of nicotine to nornicotine.

In summary, we found that CYP2A6 and CYP2B6 catalyze the nornicotine formation from nicotine in human liver microsomes. These contributions would be dependent on the individual expression levels of CYP2A6 and CYP2B6.

Acknowledgments. We acknowledge Brent Bell for reviewing the manuscript.

References

Anandatheerthavarada HK, Williams JF, and Wecker L (1993) The chronic administration of nicotine induces cytochrome P450 in rat brain. *J Neurochem* **60**:1941–1944.

Becquemont L, Le Bot MA, Riche C, Funck-Brentano C, Jaillon P, and Beaune P (1998) Use of heterologously expressed human cytochrome P450 1A2 to predict tacrine-fluvoxamine drug interaction in man. *Pharmacogenetics* **8**:101–108.

Benowitz NL (1988) Drug therapy. Pharmacologic aspects of cigarette smoking and nicotine addiction. *N Engl J Med* **319**:1318–1330.

Benowitz NL, Jacob P III, Fong I, and Gupta S (1994) Nicotine metabolic profile in man: comparison of cigarette smoking and transdermal nicotine. *J Pharmacol Exp Ther* **268**:296–303.

Broly F, Libersa C, Lhermitte M, Bechtel P, and Dupuis B (1989) Effect of quinidine on the dextromethorphan *O*-demethylase activity of microsomal fractions from human liver. *Br J Clin Pharmacol* **28**:29–36.

Crespi CL (1995) Xenobiotic-metabolizing human cells as tools for pharmacological and toxicological research. *Adv Drug Res* **26**:179–235.

Crooks PA, Li M, and Dwoskin LP (1997) Metabolites of nicotine in rat brain after peripheral nicotine administration: cotinine, nornicotine and norcotinine. *Drug Metab Dispos* **25**:47–54.

Cundy KC and Crooks PA (1984) High performance liquid chromatographic method for the determination of *N*-methylated metabolites of nicotine. *J Chromatogr Biomed Appl* **306**:291–301.

Curvall M and Kazemi Vala E (1993) Nicotine and metabolites: analysis and levels in body

fluids, in *Nicotine and Related Alkaloids: Absorption, Distribution, Metabolism and Excretion* (Gorrod JW and Wahren J eds) pp 147–179, Chapman & Hall, London.
Fukami T, Nakajima M, Yoshida R, Tsuchiya Y, Fujiki Y, Katoh M, McLeod HL, and Yokoi T (2004) A novel polymorphism of human CYP2A6 gene CYP2A6*17 has an amino acid substitution (V365M) that decreases enzymatic activity in vitro and in vivo. *Clin Pharmacol Ther* **76**:519–527.
Gervot L, Rochat B, Gautier JC, Bohnenstengel F, Kroemer H, de Berardinis V, Martin H, Beaune P, and de Waziers I (1999) Human CYP2B6: expression, inducibility and catalytic activities. *Pharmacogenetics* **9**:295–306.
Ghosheh O, Dwoskin LP, Li W, and Crooks PA (1999) Residence time and half-lives of nicotine metabolites in rat brain after acute peripheral administration of [2′-^{14}C] nicotine. *Drug Metab Dispos* **27**:1448–1455.
Ko JW, Desta Z, and Flockhart DA (1998) Human *N*-demethylation of (*S*)-mephenytoin by cytochrome P450s 2C9 and 2B6. *Drug Metab Dispos* **26**:775–778.
Kyerematen GA, Morgan ML, Chattopadhyay B, deBethizy JD, and Vesell ES (1990) Disposition of nicotine and eight metabolites in smokers and nonsmokers: identification in smokers of two metabolites that are longer lived than cotinine. *Clin Pharmacol Ther* **48**:641–651.
Lamba V, Yasuda K, Lamba JK, Assem M, Davila J, Strom S, and Schuetz EG (2004) PXR (NR1I2): splice variants in human tissues, including brain and identification of neurosteroids and nicotine as PXR activators. *Toxicol Appl Pharmacol* **199**:251–265.
Liu X, Jacob P III, and Castagnioli N Jr (1993) The metabolic fate of the minor tobacco alkaloids. in *Nicotine and Related Alkaloids: Absorption, Distribution, Metabolism and Excretion* (Gorrod JW and Wahren J eds) pp 129–145, Chapman & Hall, London.
Miksys S, Hoffmann E, and Tyndale RF (2000) Regional and cellular induction of nicotine-metabolizing CYP2B1 in rat brain by chronic nicotine treatment. *Biochem Pharmacol* **59**: 1501–1511.
Miksys S, Lerman C, Shields PG, Mash DC, and Tyndale RF (2003) Smoking, alcoholism and genetic polymorphisms alter CYP2B6 levels in human brain. *Neuropharmacology* **45**:122–132.
Miksys S and Tyndale RF (2004) The unique regulation of brain cytochrome P450 2 (CYP2) family enzymes by drugs and genetics. *Drug Metab Rev* **36**:313–333.
Murphy S, Raulinaitis V, and Brown KM (2005) Nicotine 5′-oxidation and methyl oxidation by P450 2A enzymes. *Drug Metab Dispos* **33**:1166–1173.
Nakajima M, Nakamura S, Tokudome S, Shimada N, Yamazaki H, and Yokoi T (1999) Azelastine *N*-demethylation by cytochrome P-450 (CYP)3A4, CYP2D6 and CYP1A2 in human liver microsomes: evaluation of approach to predict the contribution of multiple CYPs. *Drug Metab Dispos* **27**:1381–1391.
Nakajima M, Yamamoto T, Nunoya K, Yokoi T, Nagashima K, Inoue K, Funae Y, Shimada N, Kamataki T, and Kuroiwa Y (1996) Role of human cytochrome P4502A6 in *C*-oxidation of nicotine. *Drug Metab Dispos* **24**:1212–1217.
Newton DJ, Wang RW, and Lu AYH (1995) Cytochrome P450 inhibitors. Evaluation of specificities in the *in vitro* metabolism of therapeutic agents by human liver microsomes. *Drug Metab Dispos* **23**:154–158.
Nordberg A, Hartvig P, Lundqvist H, Antoni G, Ulin J, and Langstrom B (1989) Uptake and regional distribution of (+)-(*R*) and (−)-(*S*)-*N*-[methyl-^{11}C]-nicotine in the brains of rhesus monkey. An attempt to study nicotinic receptors *in vivo*. *J Neural Transm Park Dis Dement Sect* **1**:195–205.
Nyback H, Halldin C, Ahlin A, Curvall M, and Eriksson L (1994) PET studies of the uptake of (*S*)- and (*R*)-[^{11}C] nicotine in the human brain: difficulties in visualizing specific receptor binding in vivo. *Psychopharmacology* **115**:31–36.
Plowchalk DR, Andersen ME, and deBethizy JD (1992) A physiologically based pharmacokinetic model for nicotine disposition in the Sprague-Dawley rat. *Toxicol Appl Pharmacol* **116**:177–188.
Reidy GF, Methta I, and Murray M (1989) Inhibition of oxidative drug metabolism by orphenadrine: *in vitro* and *in vivo* evidence for isozyme-specific complexation of cytochrome P-450 and inhibition kinetics. *Mol Pharmacol* **35**:736–743.
Russell MAH and Feyerabend C (1978) Cigarette smoking: a dependence on high-nicotine boli. *Drug Metab Rev* **8**:29–57.
Soucek P (1999) Expression of cytochrome P450 2A6 in *Escherichia coli*: purification, spectral and catalytic characterization and preparation of polyclonal antibodies. *Arch Biochem Biophys* **370**:190–200.
Su T, Bao Z, Zhang QY, Smith TJ, Hong JY, and Ding X (2000) Human cytochrome P450 CYP2A13: predominant expression in the respiratory tract and its high efficiency metabolic activation of a tobacco-specific carcinogen, 4-(methylnitrosamino)-1-(3-pyridyl)-1-butanone. *Cancer Res* **60**:5074–5079.
Vial WC (1986) Cigarette smoking and lung disease. *Am J Med Sci* **291**:130–142.
Voirol P, Jonzier-Perey M, Porchet F, Reymond MJ, Janzer RC, Bouras C, Strobel HW, Kosel M, Eap CB, and Baumann P (2000) Cytochrome P-450 activities in human and rat brain microsomes. *Brain Res* **855**:235–243.
Yamanaka H, Nakajima M, Nishimura K, Yoshida R, Fukami T, Katoh M, and Yokoi T (2004) Metabolic profile of nicotine in subjects whose *CYP2A6* gene is deleted. *Eur J Pharm Sci* **22**:419–425.
Yun C-H, Shimada T, and Guengerich FP (1991) Purification and characterization of human liver microsomal cytochrome P450 2A6. *Mol Pharmacol* **40**:679–685.
Zhang Y, Jacob P III, and Benowitz NL (1990) Determination of nornicotine in smokers' urine by gas chromatography following reductive alkylation to *N′*-propylnornicotine. *J Chromatogr* **525**:349–357.

Address correspondence to: Dr. Miki Nakajima, Drug Metabolism and Toxicology, Division of Pharmaceutical Sciences, Graduate School of Medical Science, Kanazawa University, Kakuma-machi, Kanazawa 920-1192, Japan. E-mail: nmiki@kenroku.kanazawa-u.ac.jp

Available online at www.sciencedirect.com
SCIENCE DIRECT
Mutation Research 603 (2006) 64–73
Genetic Toxicology and Environmental Mutagenesis
www.elsevier.com/locate/gentox
Community address: www.elsevier.com/locate/mutres

Simultaneous measurement of gene expression for hepatotoxicity in thioacetamide-administered rats by DNA microarrays

Keiichi Minami, Rawiwan Maniratanachote, Miki Katoh, Miki Nakajima, Tsuyoshi Yokoi *

Drug Metabolism and Toxicology, Division of Pharmaceutical Sciences, Graduate School of Medical Science, Kanazawa University, Kanazawa 920-1192, Japan

Received 26 August 2005; received in revised form 26 September 2005; accepted 28 October 2005
Available online 5 December 2005

Abstract

DNA microarray technology was developed as a tool for simultaneously measuring a number of gene expression changes, and has been applied for investigations of toxicity assessments of chemicals. In this study, we used a typical hepatotoxicant, thioacetamide (TA), to find correlations between the extent of hepatotoxicity and certain gene expression patterns or specific gene expression profiles. TA was intraperitonealy administered at high (400 mg/kg), medium (150 mg/kg) or low (50 mg/kg) dose (four rats per group) and then the serum and liver were collected at the indicated time (6, 12, 24, 36 and 48 h). Serum biochemical markers were measured and hepatic mRNA expression profiles were analyzed by a DNA microarray. Serum aspartate aminotransferase (AST) and alanine aminotransferase (ALT) were increased by TA-administration in a dose-dependent manner and reached the maximum at 24 h. Hierarchical clustering analysis of all dosage groups revealed in 2 major clusters, distinguished by an early (6 and 12 h) and a late (24, 36 and 48 h) phase. The early and late phase clusters were sorted in time- and dose-dependent manners. The major gene expression profile obtained by quality-threshold (QT) clustering analysis showed the same maximal toxic time as that estimated by the serum biochemical markers. The individual expression profiles of the candidate genes selected in our previous studies and the simultaneous gene expression patterns measured by five typical hepatotoxicants including TA also reflected the hepatotoxicity of TA. These findings suggest that the potential toxic effects appearing as gene expression changes are independent of the dosage of TA. This study suggested that the major gene expression profile estimated by QT clustering would be a sensitive marker of hepatotoxicity.

Keywords: Gene expression profiles; Hepatotoxicity; DNA microarray

1. Introduction

The prediction of chemical-induced adverse effects on an organism is one of the aims of toxicology. In the past several years, a microarray technology has rapidly developed. Microarrays are available to assess both known and unknown genes in the experimental materials. Microarrays are also available to assess simultaneously the effects of various factors on the gene expression of all known sequences including expression sequence tags (ESTs) at the RNA level.

For microarray data assessment, several clustering methods are often used. Clustering places the data of interest into a small number of relatively homo-

* Corresponding author. Tel.: +81 76 234 4407; fax: +81 76 234 4407.
E-mail address: TYOKOI@kenroku.kanazawa-u.ac.jp (T. Yokoi).

1383-5718/$ – see front matter © 2005 Elsevier B.V. All rights reserved.
doi:10.1016/j.mrgentox.2005.10.008

geneous groups or clusters [1]. For example, there is hierarchical clustering expressed by a dendrogram, *K*-means clustering [2], and quality-threshold (QT) clustering [3]. These clustering methods are useful ways to extract and visualize one-to-one correlations. Microarray technology can be used as a tool for clarifying the mechanisms of chemical-induced toxicity, forecasting the adverse effects of drug candidates and improving the process of risk assessment and safety evaluation.

The liver is one of the first organs to be exposed when chemicals are administered perorally or via the portal vein. Chemical concentrations in the liver are often much higher than the peak plasma concentration. The liver is also the major site for metabolizing xenobiotics and these chemicals can lead to the formation of active metabolites. Thus, the liver is one of the primary targets for various types of chemical-induced toxicity. Therefore, investigating the gene expression changes and comparing the gene expression profiles to the extent of liver toxicity are useful for the assessment of liver toxicity.

To construct an animal model of liver toxicity, we chose thioacetamide (TA) as a potent hepatotoxicant that requires metabolic activation by mixed-function oxidases. TA is metabolized by cytochrome P450 (CYP) 2B, CYP2E1 and flavin-containing monooxygenase (FMOs) to its toxic metabolites [4,5] and these intermediate metabolites might bind to cellular proteins by the formation of acetylimidolysine derivatives [6]. The reactive metabolites responsible for TA hepatotoxicity are the radicals derived from thioacetamide-*S*-oxide and the reactive oxygen species derived as subproducts in the process of microsomal TA oxidation, both of which deplete reduced glutathione leading to oxidative stress [7–11].

The purpose of the present study is to determine the correlations between biochemical markers for hepatotoxicity and hepatic gene expression profiles at various doses of TA-administration in rats, and then to extrapolate the DNA microarray data for predicting hepatotoxic chemicals.

2. Materials and methods

2.1. Animals and chemicals

Male Sprague–Dawley rats (5-week old, 130–150 g) were obtained from SLC Japan (Hamamatsu, Japan). Animals were housed in the institutional animal facility in a controlled environment (temperature 25 ± 1 °C, humidity 50 ± 10% and 12 h light/12 h dark cycle) with access to food and water ad libitum. Animals were acclimatized for a week before use. Animal maintenance and treatment were conducted in accordance with the National Institutes of Health Guide for Animal Welfare of Japan, as approved by the Institutional Animal Care and Use Committee of Kanazawa University. TA (CAS No. 62-55-5) was obtained from Wako Pure Chemical Industries (Osaka, Japan). ISOGEN, RNA extraction reagent, was purchased from Nippon Gene (Tokyo, Japan). CodeLink™ Expression Assay Reagent kit, Manual Prep and streptavidin-Cy5 were from GE Healthcare Amersham Biosciences (Buckinghamshire, UK). The QIAquick PCR purification kit and a RNeasy mini kit were from Qiagen (Hilden, Germany). NEN Blocking Reagent and Biotin 11-UTP were from Perkin-Elmer Life Sciences (Boston, MA). ReverTra Ace (Moloney Murine Leukemia Virus Reverse Transcriptase RnaseH Minus) was from Toyobo (Tokyo, Japan). Random hexamer and SYBR® Premix Ex Taq™ (perfect real time) were from Takara (Osaka, Japan). All primers were commercially synthesized at Hokkaido System Sciences (Sapporo, Japan). Other chemicals were of the highest grade commercially available.

2.2. TA-administration and assessment of liver injury

Sixty-four rats were assigned to 16 groups (four rats/group). Rats received a single dose of TA dissolved in saline by intraperitoneal injection. The dosing solutions were prepared to deliver a volume of 2 ml/kg as follows; 400 mg/kg high dose, 150 mg/kg medium dose, 50 mg/kg low dose. At the indicated time (6, 12, 24, 36, and 48 h after the administration), blood samples were collected from the atrium, and then the rats were sacrificed and the liverscollected. Four typical biochemical markers for hepatotoxicity (aspartate aminotransferase, AST; alanine aminotransferase, ALT; lactate dehydrogenase, LDH; bilirubin) were measured by SRL (Tokyo, Japan).

2.3. RNA isolation

Total hepatic RNA was isolated using ISOGEN. Approximately 100 mg of whole liver were lysed with 1.0 ml of the reagent. Chloroform (200 μl) was added and vortexed vigorously for 15 s. The mixture was centrifuged at 15,000 × *g* for 15 min at 4 °C. The aqueous phase was transferred carefully to a new tube, and the RNA was precipitated with 0.5 ml of isopropyl alcohol for 10 min at room temperature. The mixture was centrifuged at 15,000 × *g* for 10 min. After washing with 75% ethanol, the pellet was dissolved in diethylpyrocarbonate-treated water. Equal amounts of total mRNA from samples of each administration were pooled and used for the microarray analysis and real-time reverse transcriptase (RT)-PCR.

2.4. Microarray analysis

Microarray experiments were performed using a CodeLink™ Bioarray Perfect System according to the manufacturer's protocol (GE Healthcare Amersham Biosciences). In this experiment, we used Codelink™ Uniset Rat

I Bioarray (GE Healthcare Amersham Biosciences) consisting of 9936 genes including ESTs. Processed slides were scanned with an Agilent G2565BA Microarray Scanner using Agilent Scan Control Software (Agilent Technologies, Palo Alto, CA) with the laser set to red (633 nm) and the photomultiplier tube (PMT) value to 70%. The scanned images for each slide were analyzed using the CodeLink™ Expression Analysis Software (GE Healthcare Amersham Biosciences). The microarray data quality control was as follows: present, no flags (neither marginal nor absent); marginal, low quality spots judged by analysis software; absent, low signal density spots.

2.5. Real-time RT-PCR

Rat V1a arginine vasopressin receptor (Avpr1a), cyclin G1 (Ccng1), growth arrest and DNA-damage-inducible 45alpha (Gadd45a), heme oxygenase 1 (Hmox1), L-3-hydroxyacyl-Coenzyme A dehydrogenase (Hadhsc), lysozyme (Lyz), sulfotransferase 1a2 (Sult1a2), T-cell death associated gene (Tdag) and GAPDH were quantified by real-time RT-PCR. Primer sequences used in this study were as follows: Avpr1a: 5′-TAC GTG ACC TGG ATG ACC AG-3′ and 5′-AGC AAC GCC GTG ATT GTG AT-3′ [12], Ccng1: 5′-CCT TCC AAT TTC TGC AGC TC-3′ and 5′-CTT GGA AAC AAG CTC TTG CC-3′ [13], Gadd45a: 5′-AAG ATC GAA AGG ATG GAC ACG-3′ and 5′-GTA GCA ACA GCT CTG CCA GC-3′ [14], Hmox1: 5′-ATA GAG CGA AAC AAG CAG A-3′ and 5′-TAG AGC TGT TTG AAC TTG G-3′, Hadhsc: 5′-TGC AGA TCA CAA ACA TAG CC-3′ and 5′-TCC AGT CCA ACA TAG TCA AG-3′, Lyz: 5′-CTC AAA CCA ACA GGG CTT TC-3′ and 5′-CCC AAG ATC AAC TCG TCT CC-3′ [15], Sult1a2: 5′-TCA TTG AGT GGA CTT TGC CTT-3′ and 5′-CAC TTT TCC AGC TTT GAA CTG-3′, Tdag: 5′-CCA AGC AGG TAC AAC ATC AG-3′ and 5′-TTC TGC CTC GTA GAC TTG AC-3′, GAPDH: 5′-GTT ACC AGG GCT GCC TTC TC-3′ and 5′-GGG TTT CCC GTT GAT GAC C-3′. For RT process, total RNA (4 μg) and 150 ng random hexamer were mixed and incubated at 70 °C for 10 min. The RNA solution was added to a reaction mixture containing 100 units of ReverTra Ace, reaction buffer and 0.5 mM dNTPs in a final volume of 40 μl. The reaction mixture was incubated at 30 °C for 10 min, 42 °C for 1 h and heated at 98 °C for 10 min to inactivate the enzyme. Real-time PCR was performed using the Smart Cycler® (Cepheid, Sunnyvale, CA) with Smart Cycler® software (Ver. 1.2b). The PCR mixture contained 1 μl of template cDNA, SYBR® Premix Ex Taq™ solution and 10 pmol of sense and antisense primers. The PCR condition for Ccng1, Sult1a2 and GAPDH was as follows: after an initial denaturation at 95 °C for 30 s, the amplification was performed by denaturation at 94 °C for 4 s, annealing and extension at 64 °C for 20 s for 45 cycles. The PCR condition for other six genes was as follows: after an initial denaturation at 95 °C for 20 s, the amplification was performed by denaturation at 95 °C for 5 s, annealing at 55 °C for 10 s and extension at 72 °C for 15 s for 45 cycles. The amplified products were monitored directly by measuring the increase of the dye intensity of the SYBR® Green I.

2.6. Data management

Microarray data management was performed with GeneSpring software (Agilent Technologies). Comparison of present genes, fold change determinations, experiment normalization and various clustering analyses were performed. The gene expression values for each array were normalized to their respective median value. All clustering analyses were performed using standard correlations. Fold change filters included the requirement that the genes be present in at least 200% of controls for up-regulated genes and lower than 50% of controls for down-regulated genes.

3. Results

3.1. Assessment of liver toxicity

The serum biochemical markers in the TA-administered groups were measured at 6, 12, 24, 36 and 48 h after administration (Fig. 1). The AST activities of all dosage groups were significantly high at 24 h. The changes of ALT activities were similar to those of the AST activities. The LDH activity increased significantly in the medium dose- and the high dose-administered groups at 24 h, but not in the low dose-administrated groups. No significant change of the unconjugated bilirubin was observed in any of the groups (data not shown), whereas conjugated bilirubin increased only in the 24 h high-dose group (0 h: 0 mg/dl, 24 h: 0.3 mg/dl). Taking these results into consideration, the maximal toxic times of each TA dosage were estimated as 24 h.

3.2. Two-way hierarchical clustering of gene expression profiles in TA-induced hepatotoxicity in rats

The mRNA expression profiles in the three dosage and five time points were determined using the data from the DNA microarray. Two-way hierarchical clustering was performed based on the expression profiles of the genes with a significant variation in the expression level across all the experiments. After cutting off the absent and marginal flags, 7978 out of 9936 genes were present in this experiment. The results are shown in a color-coded matrix (Fig. 2) where samples are ordered on the horizontal axis and genes on the vertical axis on the basis of the similarity of their expression profiles.

The administered groups were sorted into two large clusters that extensively differed with respect to an early phase (6 and 12 h; left cluster) or a late phase (24, 36 and 48 h; right cluster) (Fig. 2A). In the early phase cluster,

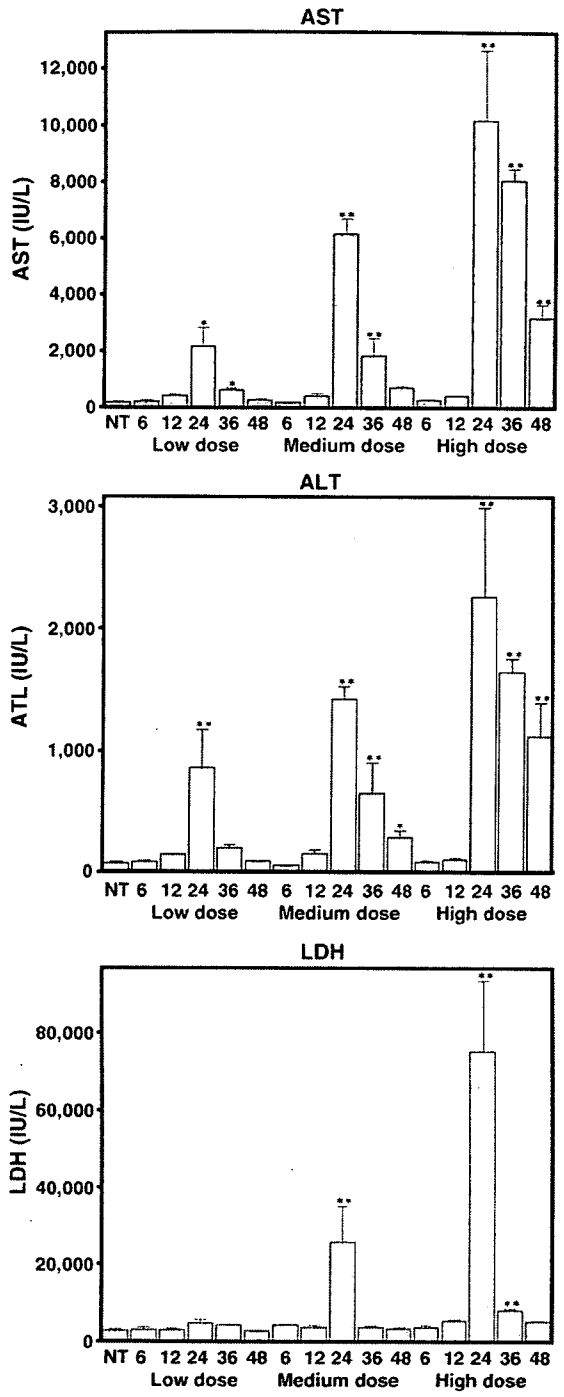

Fig. 1. Changes of AST, ALT and LDH in serum of TA-administered rats. TA was administered at high dose (400 mg/kg weight), medium dose (150 mg/kg weight) and low dose (50 mg/kg weight). Blood samples were collected at 6, 12, 24, 36, 48 h after administration. Data are expressed as mean ± S.E. from four rats. Significantly different from NT group ($^{*}p<0.05$, $^{**}p<0.01$). NT; non-treated.

Table 1
Classification of genes those expression were significantly changed in all TA-administered groups

Category	Total[a]	Present[b]	Up (%)	Down (%)
Apoptosis regulator	33	25	4 (16.0)	0 (0)
Cancer	51	28	3 (10.7)	0 (0)
Cell cycle regulator	25	19	2 (10.5)	1 (5.3)
Chaperone	33	19	1 (5.3)	2 (10.5)
Enzyme	852	657	24 (3.7)	100 (15.2)
Immunity protein	42	31	0 (0)	2 (6.5)
Microtublar protein	16	8	0 (0)	1 (12.5)
Nucleic acid binding	175	126	12 (9.5)	6 (4.8)
Other groups	102	71	2 (2.8)	1 (1.4)
RNA	2	1	0 (0)	0 (0)
Signal transducer	201	124	7 (5.6)	9 (7.3)
Storage	3	2	0 (0)	0 (0)
Structural protein	181	116	7 (6.0)	12 (10.3)
Transport	313	208	10 (4.8)	26 (12.5)
Total	2029	1435	72 (5.0)	160 (11.1)

Up-regulated gene showed more than 200% expression of control. Down-regulated gene showed less than 50% expression of control.
[a] Gene number those category were defined.
[b] Gene number showing enough spot density.

the 12 h-groups were sorted into small hierarchies. On the other hand, the late phase cluster groups were sorted in a dose-dependent manner except for the 24 h-group. Especially, all dosages in the 24 h-groups were categorized at the same level.

We also performed hierarchical clustering based on each dosage (Fig. 2B). The clusters were sorted in a similar pattern as shown in Fig. 2A. The distance between the early (6 and 12 h) and the late (24, 36 and 48 h) phase was increased in a time-dependent manner as shown in the dendrogram of each group (above the matrix, Fig. 2B).

3.3. *Category classification of genes in TA-induced hepatotoxic Rats*

To evaluate the gene expression pattern on the basis of gene function, we classified the genes whose expressions were significantly changed at all dosages in the 24 h groups (Table 1). Based on each gene annotation, 13 categories were classified. Based on the percentage and the gene numbers categorized by gene annotation, the genes in the apoptosis regulator and the nucleic acid binding category were typically up-regulated and the genes in the enzyme, structural protein and transport category were down-regulated (Table 1).

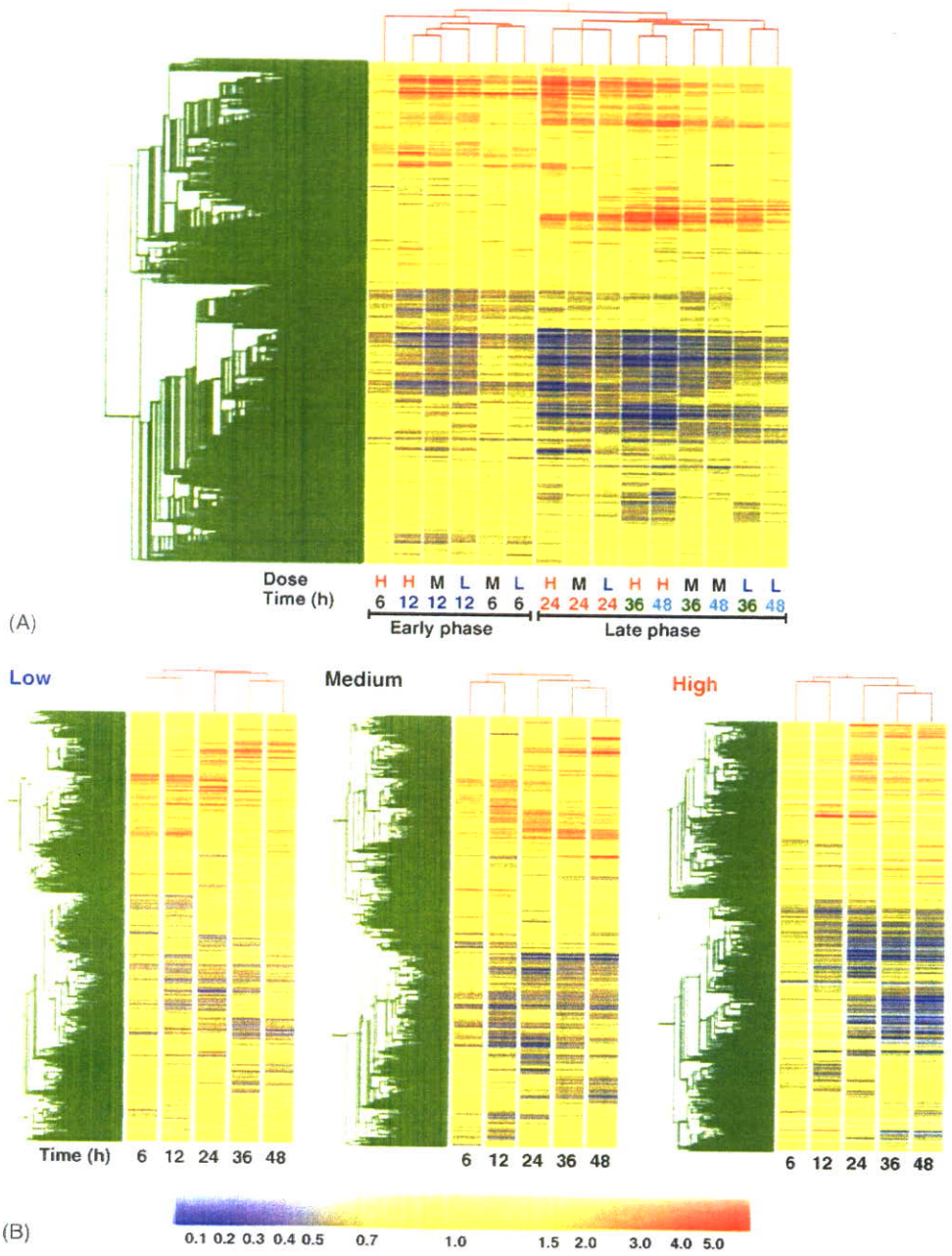

Fig. 2. Two-way hierarchical clustering analyses of hepatic gene expression profiles. Hierarchical clustering of all groups (A) and each dosage group (B). Data of 7978 genes are expressed in a color-coded matrix. Red- and blue-color in matrix indicate the expression levels of above and below the median, respectively. Dendrograms of each group (above the matrix, red lines) and gene (left of the matrix, green lines) represent the overall similarities in gene expression profiles. H: high dose (400 mg/kg); M: medium dose (150 mg/kg); L: low dose (50 mg/kg).

3.4. QT clustering analysis based on the dose of TA

QT clustering analysis was performed in order to estimate the major gene expression profiles based on the TA dosage (Fig. 3). In this process, we used GeneSpring QT clustering algorism. In all dosage groups, we selected the highest correlation coefficient that identified both the up- and the down-regulated types of cluster. The analysis setting for the minimal cluster size was 1000 genes and the minimal correlation coefficients of the 6, 12, 24, 36, and 48 h groups were 0.82, 0.92, 0.91, 0.88 and 0.86, respectively. The probe sets used in this clustering were the same as those used in the hierarchical clustering (7978 of 9936 genes). In the up-regulated

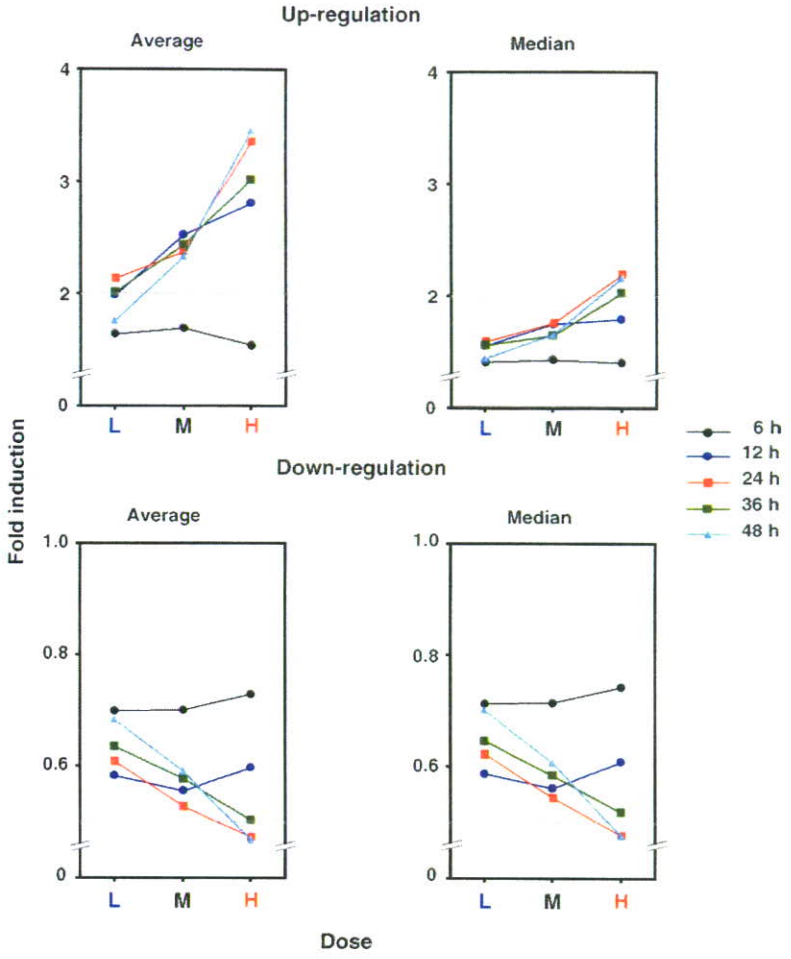

Fig. 3. QT clustering analyses based on the dose of TA. Groups at 6, 12, 24, 36, and 48 h after administration were evaluated and expressed as average (left) or median (right) values. Analysis settings are described in Section 3. Minimal correlation coefficients selected in this analysis were as follows: 6 h, 0.82; 12 h, 0.92; 24 h, 0.91; 36 h, 0.88; 48 h, 0.86. H: high dose; M: medium dose; L: low dose.

cluster, the gene numbers of each time group were as follows: 6 h, 1028; 12 h, 1010; 24 h, 1003; 36 h, 1008; 48 h, 1000. In the down-regulated cluster, the gene numbers of each time group were as follows: 6 h, 1903; 12 h, 1724; 24 h, 1546; 36 h, 1533; 48 h, 1513. The expression changes of these genes in each dosage group are shown as average and median values (Fig. 3). As a result, both the average and the median of the gene expression profiles before 12 h showed no difference between the three dosage groups. However, the gene expression profiles after 24 h of administration changed in a dose-dependent manner.

3.5. *QT clustering analysis based on the time after TA-administration*

QT clustering analysis was performed in order to estimate the major gene expression profiles based on the time after TA-administration (Fig. 4). In the low-limited correlation analysis, we selected the highest correlation coefficient that identified the up- and down-regulated type of clusters. The low-limited analysis setting for the minimal cluster size was 1000 genes and the minimal correlation coefficients of the low-, medium- and high-dose groups were 0.68, 0.58, and 0.47, respectively. The probe sets used in this clustering were the same as those used in the hierarchical clustering (7978 of 9936 genes). In the up-regulated type cluster, the low-, medium- and high-dose groups contained 1021, 1003 and 1000 genes, respectively (Fig. 4A). The down-regulated type cluster of the low-, medium- and high-dose groups contained 2129, 2050 and 1606 genes, respectively (Fig. 4B). In the high-limited correlation analysis, we selected the highest correlation coefficient that identified only one dominant cluster (Fig. 4C). The high-limited correlation analysis setting for the minimal cluster size was 1000 genes and

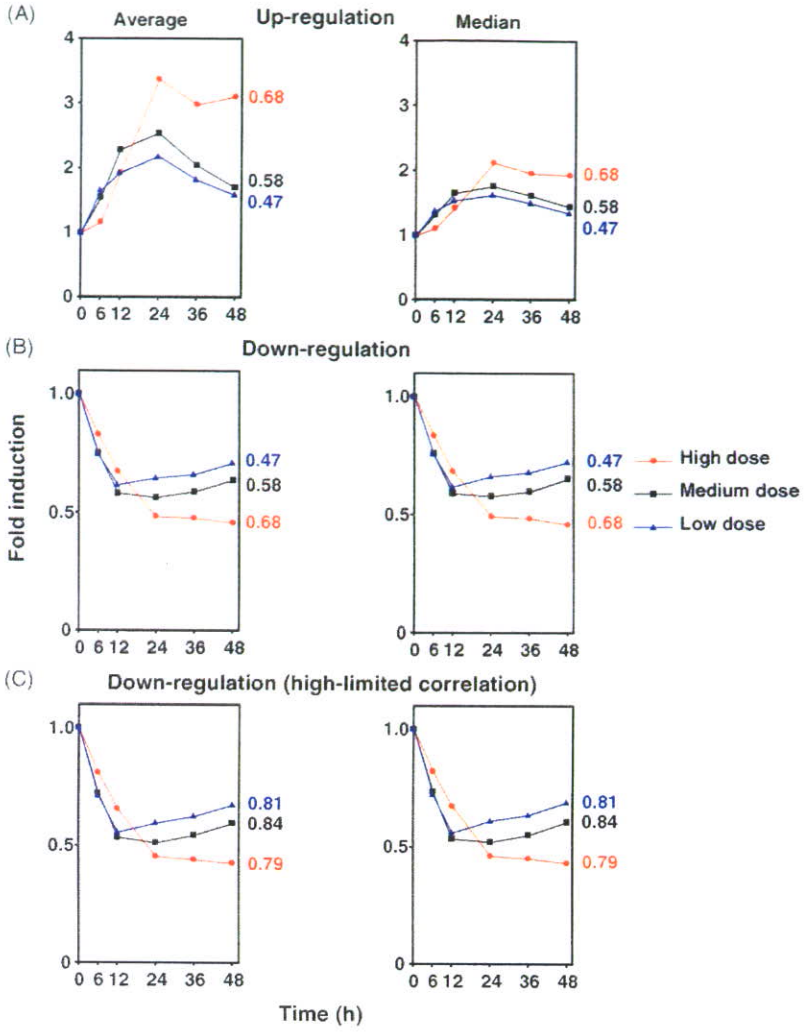

Fig. 4. QT clustering analyses based on the time after TA-administration. Groups at 6, 12, 24, 36, and 48 h after administration were evaluated with low (A and B)- and high (C)-limited correlation coefficients. Analysis settings are described in Section 3. Data are expressed as average or median values of these clusters. The minimal correlation coefficients selected in this analysis were as follows: low-limited correlation: high dose, 0.68; medium dose, 0.58; low dose, 0.47 (A and B). High-limited correlation: high dose, 0.79; medium dose, 0.84; low Dose, 0.81 (C).

the minimal correlation coefficients of the low-, medium- and high-dose groups were 0.79, 0.84 and 0.81, respectively (Fig. 4C). In the down-regulated type cluster, the low-, medium- and high-dose groups contained 1016, 1002 and 1016 genes, respectively (Fig. 4C). Both the average and median values of the QT clustering and the expression profiles of almost all dosage groups demonstrated peak values at 24 h after administration, which was the same as the maximal toxic time. Independently of the extent of toxicity, the major gene expression profiles based on the time after TA-administration showed almost the same pattern. However, the changes of the up- and down-regulated genes occurred in a dose-dependent manner.

3.6. Toxicity marker analysis

Previously, in rats we identified potential hepatotoxic marker genes from five hepatotoxicants (acetaminophen, bromobenzene, carbon tetrachloride, dimethylnitrosamine and TA) by using cDNA microarray [16]. The up- and down-regulated groups consisted of nine and seven genes, respectively (Fig. 5). In the present study, changes in the expression of potential hepatotoxic marker genes were demonstrated. As shown in Fig. 5, the maximal up- or down-regulated time points in almost all the individual gene expression profiles reflected the maximal toxic time. In addition, the individual gene expression profiles of each dosage showed similar patterns. In